eLife

Reviewed Preprint
v2 • August 13, 2024
Revised by authors

Reviewed Preprint
v1 • December 27, 2023

Stem Cells and Regenerative Medicine

Epigenetic insights into GABAergic development in Dravet Syndrome iPSC and therapeutic implications

Jens Schuster, Xi Lu, Yonglong Dang, Joakim Klar, Amelie Wenz, Niklas Dahl, Xingqi Chen

Department of Immunology, Genetics and Pathology, Uppsala University and Science for Life Laboratory, Uppsala, Sweden

Abstract

Dravet syndrome (DS) is a devastating early onset refractory epilepsy syndrome caused by variants in the *SCN1A* gene. A disturbed GABAergic interneuron function is implicated in the progression to DS but the underlying developmental and pathophysiological mechanisms remain elusive, in particularly at the chromatin level. In this study, we utilized induced pluripotent stem cells (iPSCs) derived from DS cases and healthy donors to model disease-associated epigenetic abnormalities of GABAergic development. Employing the ATAC-Seq technique, we assessed chromatin accessibility at multiple time points (Day 0, Day 19, Day 35, and Day 65) of GABAergic differentiation. Additionally, we elucidated the effects of the commonly used anti-seizure drug valproic acid (VPA) on chromatin accessibility in GABAergic cells. The distinct dynamics in chromatin profile of DS iPSC predicted accelerated early GABAergic development, evident at D19, and diverged further from the pattern in control iPSC with continued differentiation, indicating a disrupted GABAergic maturation. Exposure to VPA at D65 reshaped the chromatin landscape at a variable extent in different iPSC-lines and rescued the observed dysfunctional development in some DS iPSC-GABA. This study provides the first comprehensive investigation on the chromatin landscape of GABAergic differentiation in DS-patient iPSC, offering valuable insights into the epigenetic dysregulations associated with interneuronal dysfunction in DS. Moreover, our detailed analysis of the chromatin changes induced by VPA in iPSC-GABA holds the potential to improve development of personalized and targeted anti-epileptic therapies.

eLife assessment

This is a potentially **useful** study that shows changes in the chromatin landscape of GABAergic neurons in induced pluripotent stem cells (iPSCs) derived from both Dravet Syndrome (DS) patients and healthy donors. The strength of the evidence is currently **incomplete** because the authors compared iPSCs from different individuals, rather than isogenic controls. A strategy for minimizing variability across cell lines is used, but the explanation is not complete. The revised manuscript adds RNAseq and qPCR measurements of the expression of the gene SCN1A, however these do not appear to agree, perhaps because of the way the qPCR measurements are normalized, and there is no measurement of Nav1.1, the gene product thought to be responsible for the majority of DS cases. Hence the evidence that there is reduced expression of SCN1A or its gene product is not complete and therefore it is difficult to evaluate whether or not the observed epigenetic changes are causal. The work would potentially be of interest to scientists who study development, developmental disorders, and epigenetic contributions to disease.

https://doi.org/10.7554/eLife.92599.2.sa2

Introduction/Background

Dravet syndrome (DS) is an early onset and intractable epilepsy with an unfavorable long-term outcome. The first seizures are usually triggered by fever within the first 12 months of life[1,2]. Characteristic clinical features are age-related progression of seizures, cognitive decline, behavioral problems and movement disorder. The complex neurological symptoms associated with DS suggest underlying pathophysiological mechanisms that interfere with brain development[1–4]. Approximately 80% of DS cases carry heterozygous variants in the *SCN1A* gene encoding the α-subunit voltage-gated sodium channel (Nav1.1)[1,5]. Prior insights on the neuropathophysiology in DS have come from the *Scn1a* heterozygous mice, indicating a vital role of cortical interneurons in the pathogenesis. Mice with Nav1.1 haploinsufficiency in GABAergic interneurons exhibit spontaneous seizures and behavioral abnormalities[6–9] that are associated with subnormal sodium currents and impaired excitability of inhibitory interneurons[10,11]. Additionally, human iPSC derived neural cells carrying distinct pathogenic *SCN1A* variants have recapitulated electrophysiological and molecular perturbations in DS[12–16]. In combination, these studies have confirmed that *SCN1A* variants cause delayed sodium currents in activated and mainly inhibitory GABAergic interneurons, supporting the notion that seizures in DS are caused by deficient cortical inhibition[12].

Interneuronal progenitors emerge from the embryonic subpallium, mainly the median ganglionic eminence, and migrate tangentially to cortical progenitor zones. The second half of gestation is a period of rapid development of the human cortical GABAergic system that continues after term[17,18]. The extended developmental processes into mature GABAergic interneurons require continuous and complex remodeling of the chromatin structure for transcriptional adaptations[19]. While it is now clear that the distinct features in DS is associated with a reduced sodium current density in Nav1.1 haploinsufficient interneurons and a disinhibition of the cortical network[6,13,20], the underlying epigenetic mechanisms are poorly understood.

Treatment of DS patients is challenging and seizure control is rarely attainable[21]. The most frequently used first-line drug is valproic acid (VPA)[1]. However, more than 50% of DS patients are drug resistant without any decrease in seizure-frequency upon treatment[1], indicating

endogenous and subject-specific responses to VPA. The mechanisms by which VPA act are not fully understood, but studies suggest that the drug inhibits histone deacetylase (HDAC) with an impact on chromatin structure and gene expression[22,23]. Furthermore, a direct interaction of VPA with sodium- or calcium-gated ion channels (e.g. Nav1.1) and enzymes crucial for GABA turnover has been proposed[22]. While these studies have brought important information on the mode of action of VPA[24–28], the specific effects of VPA on chromatin architecture of inhibitory GABAergic interneurons have not yet been investigated to our knowledge.

We recently established induced pluripotent stem cell (iPSC) lines carrying distinct disease-causing variants in the *SNC1A* gene and modeled GABAergic interneuron development in DS[13,29]. The DS-patient iPSC derived GABAergic neurons recapitulated electrophysiological abnormalities and gene expression analysis showed enrichment for histone modifications, suggesting epigenetic abnormalities[13]. We therefore sought to explore the dynamics of open chromatin in our DS-model of GABAergic development in DS using the assay of transposase accessible chromatin sequencing (ATAC-Seq). The methodology has previously been used to study chromatin accessibility of annotated genes during brain development[30–32] and, specifically, in interneuronal differentiation[19,33]. Herein, we employed ATAC-Seq to investigate the dynamics of chromatin accessibility in iPSC of DS-patients and healthy donors at four different time points (Day 0, Day 19, Day 35, and Day 65) of GABAergic development. Moreover, we explored the effect of VPA on chromatin accessibility in GABAergic neurons. Our study uncovered accelerated chromatin changes in DS patient cells during the initial phase of GABAergic development (up to Day 19) when compared to cells of healthy donors. Further differentiation revealed that DS-patient GABAergic cells acquire a distinct chromatin profile when compared to that of control cells. Notably, VPA treatment of GABAergic neurons leads to unspecific genome-wide changes in chromatin architecture that predicts a promoted GABAergic development in some iPSC lines. This study represents the first investigation of the chromatin dynamics of GABAergic development in DS-patient iPSC, shedding light on the underlying epigenetic abnormalities. Moreover, the in-depth characterization of chromatin changes in GABAergic neurons induced by VPA may bring important information for the development of individualized anti-seizure therapies.

Results

Dynamic chromatin accessibility in an iPSC model of GABAergic development

We previously established a protocol for GABAergic interneuronal differentiation of iPSC[13,29]. Analysis of RNAseq data at D19 and D65 of GABAergic differentiation revealed *SCN1A* expression in neuronal cells derived from healthy donors and from patients with Dravet disease (**Supplementary Figure 1A**). The *SCN1A* expression was confirmed with qPCR at D19, D35, and D65 of differentiation whereas no expression could be detected in undifferentiated iPSC (D0; **Supplementary Figure 1B**). We then applied ATAC-Seq to investigate the dynamics of chromatin accessibility in GABAergic development associated with *SCN1A* variants. We first obtained a reference for chromatin accessibility changes during GABAergic interneuronal differentiation in iPSC from three healthy donors (Ctl) using ATAC-Seq[35] (**Figure 1A**). The differentiating cultures were collected at four distinct time points of differentiation at day 0 (D0; termed iPSC), D19 (neural progenitor cells; NPC), D35 (intermediate neuronal cells; imN) and D65 (GABAergic interneurons; GABA). The cultures displayed expression of marker genes confirming the development into GABAergic interneurons[13]. As previously shown, cultures stained positive for pluripotent stem cell markers such as NANOG, SOX2, and OCT4 at D0. The expression of these markers decreased upon neural induction and disappeared with further differentiation. Markers for neural progenitor cells (FOXG1, PAX6) were expressed at D19 followed by the expression of immature neuronal cell markers (DCX and NKX2.1) at D35 and of markers for GABAergic interneurons (GAD1, TUBB3) at D65 (**Supplementary Figure 1C and Schuster et al. 2019**[13]).

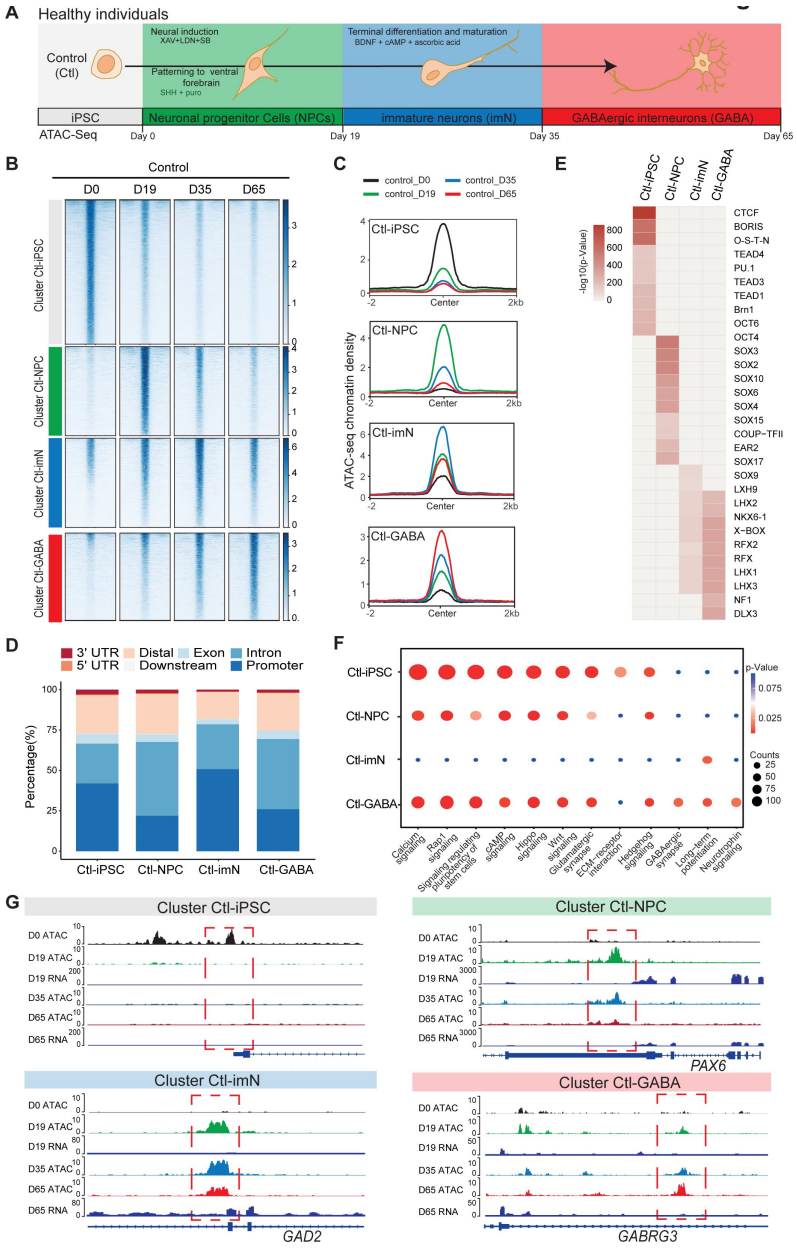

Figure 1

Chromatin accessibility dynamics during GABAeric interneuron differentiation of control iPSCs

A. Schematic illustration of GABAergic interneuron differentiation protocol. Cells from iPSC differentiation were collected for ATAC-Seq. Interneuron differentiation was grouped into four stages: iPSC (Day 0), neural progenitor cells; NPCs (Day 19), immature neurons, imN (Day 35), GABAergic interneurons, GABA (Day 65).

B. Heatmap of four Clusters identified by time series analysis using temporal changes in chromatin accessibility compared to D0 (Day 0) and other points. The signal strengths were denoted by color intensities.

C. Line plots showing chromatin accessibility at cluster-specific regions from each time point.

D. Barplot for genomic distribution of differential chromatin accessible regions for each cluster.

E. Heatmap for top 10 TFs enrichment in each cluster. The significance was denoted by color intensities. O-S-E-N = OCT4-SOX2-TCF-NANOG.

F. Bubble plot of KEGG pathway enrichment for each cluster. p-value and enrichment were indicated. The corresponding comprehensive list of enrichment terms can be found in Supplementary Table 2.

G. Genome browser view showing representative differential chromatin accessible regions at the indicated gene loci. Additionally, RNA-seq data[13] is visualized at D19 and D65.

The quality of ATAC-Seq data from each sample was validated by sequencing depth comparison, genome-wide correlation between technical replicates and by calculating the fraction of reads in enriched peaks (FRiP), the transcription start site enrichment score (**Supplementary Figure 2A**-D). We captured accessible chromatin peaks at each time-point of differentiation: 58,382 peaks at D0 (Ctl-iPSC), 68,002 peaks at D19 (Ctl-NPC), 52,933 peaks at D35 (Ctl-iMN), and 74,561 peaks at D65 (Ctl-GABA) (**Supplementary Table 1**). Genomic annotation of the accessible chromatin sites with respect to promoters, introns and exons revealed a heterogenous distribution in iPSC, NPC, imN and GABA (**Supplementary Figure 2E**). Furthermore, principal component analysis (PCA) of chromatin accessibility at the four time points demonstrated that the three biological replicates separated into four clusters corresponding to each of the four time points of GABAergic development (**Supplementary Figure 2F**), albeit with some degree of variability at the intermediate time points (D19 (NPC) and D35 (imN)), possibly reflecting cell line specific and endogenous differences reported previously[36]. We therefore treated the three Ctl-iPSC-lines as biological replicates for downstream analysis. We also performed genome-wide correlation of ATAC-Seq with our previously published RNA-Seq data at D19 and D65 (**Supplementary Figure 2G**). The correlation ranged between 0.52 and 0.57, further indicating the good quality of the ATAC-Seq data.

We then characterized changes in chromatin accessibility during GABAergic development in Ctl-iPSC. The ATAC-Seq peaks in iPSC (D0) were used as reference and compared to the accessible peaks in NPC, imN and GABA. To avoid capturing the dynamic changes of accessible regions caused by variability across individuals, we initially compared the dynamic changes of chromatin accessibility cell line by cell line across differentiation. Subsequently, we extracted the common changes observed across different cell lines at each time point (**Methods**). In total, we identified 19,931 significant differential peaks (|log2(fold change (FC))| > 1, false discovery rate (FDR) < 0.01) (**Supplementary Figure 3A, Methods**). Next, we employed an unbiased cluster method to investigate the dynamics of these differential accessible peaks, resulting in the identification of four distinct clusters (Cluster 1-4) (**Figure 1B, Supplementary Figure -3B-D**). Cluster 1 (n=9,565) consisted of peaks that were open D0 (cluster Ctl-iPSC) and that gradually closed during differentiation. Cluster 2 (n=3,285) contained peaks that were predominantly open at D19 (cluster Ctl-NPC). Cluster 3 (n=3,533) exhibited a high chromatin accessibility at both D19 and D35 (cluster Ctl-imN) but more closed at D65. Cluster 4 (n=3,545) displayed the highest accessibility specifically at D65 (cluster Ctl-GABA; **Figure 1B, 1C**). A genomic annotation of the differential peaks in the four clusters with respect to promoters, exons, introns and distal regulatory sequences revealed differences mainly in introns and promoter regions. The Ctl-NPC cluster and Ctl-GABA cluster showed the highest proportion of open chromatin in introns (45.6% and 43.4%, respectively) whereas in the Ctl-iPSC and Ctl- imN clusters most accessible peaks were located in promoter regions (41.9% and 50.8%, respectively; **Figure 1D**).

We then performed transcription factor (TF) enrichment analysis on the differential peaks specific to each cluster (**Figure 1E**). The Ctl-iPSC cluster showed specific enrichment for motifs of TFs for pluripotency, such as BRN1, OCT6, among others (**Figure 1E**), whereas motifs for the SOX family of TFs were enriched in the Ctl-NPC-cluster. Ctl-NPC-specific transcription factor motifs (e.g., SOX family TFs) were detected in the NPC-specific cluster. Notably, motifs for common TFs (e.g., LHX family TFs, NKX6, RFX) as well as unique TFs

(e.g. SOX9, NF1 and DLX3) were enriched in both the Ctl-imN-specific cluster and the Ctl- GABA specific cluster. The SOX family of TFs are important regulators of neuronal development[37] and DLX factors function in orchestrating transcriptional activity during cortical GABAergic development[38]. The temporal pattern of accessible and enriched TF motifs in our differentiating Ctl-iPSC cultures is thus consistent with the TFs required for neuronal and cortical GABAergic development *in vivo*, confirming our model system to be relevant.

Furthermore, we examined the biological processes associated with each cluster by assigning each differential peak to the nearest gene. The annotated genes were then used for KEGG analysis of each cluster (**Figure 1F**, **Supplementary Table 2**). In the Ctl-iPSC cluster we identified enrichment of pathways related to pluripotency, such as signaling regulating pluripotency of stem cells, while the Ctl-GABA cluster showed exclusive enrichment for pathways for GABAergic neurons, such as GABAergic synapse and Neurotrophin signaling (**Figure 1F**). Genome traces of annotated genes in each cluster validated the differential accessible chromatin, e.g. for *NANOG* in the Ctl-iPSC cluster, *PAX6* and *GAD2* in the Ctl-NPC and Ctl-imN clusters, respectively, and *GABRG3* in the Ctl-GABA cluster (**Figure 1G**). Gene expression analysis of RNA-seq data at D19 and D65, as well as with qPCR at D0, D19, D35, and D65, indicated that expression levels of the four genes was consistent with the chromatin accessibility patterns (**Supplementary Figure 3E**). Taken together, these findings show that the captured chromatin dynamics comply with the induction and development of GABAergic neurons.

Dynamic chromatin accessibility in a DS-iPSC model of GABAergic development

Next, to gain a deeper understanding of chromatin dynamics during GABAergic development associated with DS, we used the same strategy as above for differentiation and ATAC-Seq analysis of iPSC-lines derived from the three DS patients (**Figure 2A**, **Supplementary** Figure 4). Unfortunately, one of the DS-iPSC lines (DD4A) did not differentiate up to D65 for unknown reasons why data at this specific time-point are based on two DS-iPSC lines.

The ATAC-Seq data showed high quality and reproducibility at all four time-points (**Supplementary Figure 4A**-D). In total, we detected 89,363 peaks in DS-iPSC, 79,270 peaks in DS-NPC, 113,519 peaks in DS-imN, and 41,665 peaks in DS-GABA (**Supplementary Table 3**). The genomic distribution of these accessible chromatin peaks with respect to promoters, introns and exons showed deviations when compared to Ctl-iPSC lines, mainly at D35 (DS-imN) and at D65 (DS-GABA) (**Supplementary Figure 4E**). Furthermore, the PCA of chromatin accessibility in DS-iPSC replicates showed that they clustered together at D0, D19 and D35 (**Supplementary Figure 4F**). Notably, the clusters at D19 (iPSC-NPC) and at D35 (iPSC-imN) showed a strong overlap in contrast to the well distributed clusters at all four time points in Ctl-iPSC lines (**Supplementary Figure 2F** and 4F). Genome-wide correlation of ATAC-Seq and RNA-seq data at D19 and D65 showed good correlation (0.49 to 0.55; **Supplementary Figure 4G**). The different dynamics of chromatin accessibility of DS-iPSC lines when compared to that of Ctl-iPSC lines thus suggest a disrupted developmental trajectory into DS-GABAergic interneurons consistent with an altered function of inhibitory GABAergic interneurons in *Scn1a* heterozygous mice.

To further characterize chromatin changes in GABAergic differentiation of DS-iPSC lines, we used the same strategy as for Ctl-iPSC lines by using the profile of chromatin accessibility in DS-iPSCs (D0) as a reference. To avoid capturing the dynamic changes of accessible regions caused by variability across individuals, we applied the same strategy as described for the control samples (Methods). In total, we identified 19,896 differential peaks ($|\log2(FC)| > 1$, FDR < 0.01) (**Methods**) that were clustered into four groups using an unbiased approach. The four DS-specific clusters showed similar patterns as those of the Ctl group. The number of accessible peaks were 8,517 at D0 (DS-iPSC), 4,317 at D19 (DS-NPC), 3,579 at D35 (DS-imN) and 3,483 at D65 (DS-GABA) (**Figure 2B**, **2C, Supplementary** Figure 5A-D). We identified differences in the genomic distribution of the DS-iPSC clusters when compared to that in the Ctl-iPSC clusters (**Figure 1D**, **2D**). In the control group, 42.0% of the peaks were located in promoter regions, whereas in the patient group, this proportion was slightly lower at 37.3%. Additionally, a slightly higher proportion of DS-iPSC specific peaks were found in intron regions (26.5%) compared to Ctl-iPSC (24.6%). The genomic features of the DS-NPC specific cluster were similar between the Ctl group and the DS group. In the DS-imN specific cluster, a lower proportion of peaks were located in promoter regions when compared to that of the Ctl group (50.8% vs. 23.1%), while a lower proportion of peaks were from

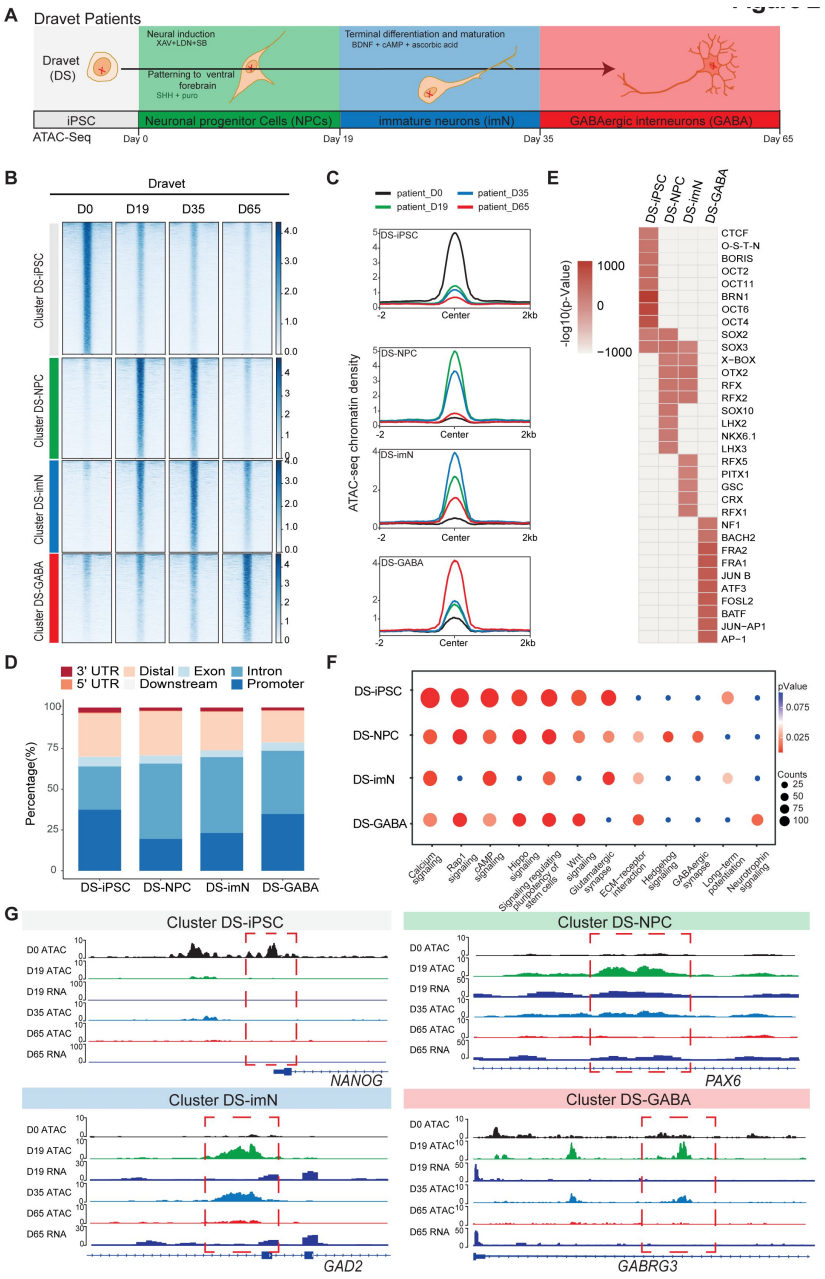

Figure 2

Chromatin accessibility dynamics during GABAergic differentiation of Dravet Syndrome patient iPSCs

A. Schematic Illustration of the design for GABAergic differentiation in Dravet syndrome patients. Cells from iPSC differentiation were collected for ATAC-Seq. GABAergic differentiation in Dravet Syndrome patients was grouped into four stages: iPSC (Day 0), NPCs (Day 19), imN (Day 35), GABA(Day 65).

B. Heatmap of four clusters identified by time series analysis using temporal changes in chromatin accessibility compared D0 (Day 0) and other points. The signal strengths were denoted by color intensities

C. Line plots showing chromatin accessibility at cluster-specific regions from each time point.

D. Barplot for genomic distribution of differential chromatin accessible regions for each cluster.

E. Heatmap for top 10 TFs enrichment in each cluster. The significance was denoted by color intensities. O-S-E-N = OCT4-SOX2-TCF-NANOG.

F. Bubble plot of KEGG pathway enrichment for each cluster. p-value and enrichment were indicated. The corresponding comprehensive list of enrichment terms can be found in Supplementary Table 4.

G. Genome browser view showing representative differential chromatin accessible regions at the indicated gene loci. Additionally, RNA-seq data[13] is visualized at D19 and D65.

intron regions in the Ctl group (27.8%) when compared to the DS group (46.2%). In the DS-GABA and Ctl-GABA specific clusters, 34.7% and 25.9% of the peaks were located in promoter regions, respectively, while 38.7% and 43.4% of the peaks were in intron regions in the Ctl and DS groups, respectively.

We then examined the enrichment of motifs for trans-acting TFs within the differential peaks of each DS-cluster at each time-point (**Figure 2E**). The DS-iPSC cluster specific peaks showed enrichment of motifs from pluripotency related TFs, such as BRN1 and OCT4, whereas TF motifs for the SOX family of TFs were enriched in both the DS-iPSC cluster and DS-NPC cluster (**Figure 2E**). Peaks at TF motifs for LHX3 and NKX, specific for GABAergic neurons were enriched only in the DS-NPC cluster but not in the DS-GABA cluster. However, the DS- GABA specific peaks were enriched at motifs for the activator protein-1 (AP-1) family of TFs, including JUN, FRA, and FOSL. Enriched motifs for the BACH2 TF were observed only in the DS-GABA specific peaks and not in the Ctl-GABA peaks. Together, these data further support that DS-iPSC, although they initially respond to our protocol for GABAergic induction with accessible motifs for the SOX family of TFs, have a disrupted trajectory into GABAergic interneurons as shown by the loss of motifs for DLX and LHX at D65.

Next, we annotated the differential accessible peaks to nearby genes and performed KEGG pathway analysis for each cluster (**Figure 2F**, **Supplementary Table 4**). Similar to Ctl-iPSC, the peaks of the DS-iPSC specific cluster were enriched for pathways related to pluripotency. However, and in contrast to the control group, pathways related to GABAergic synapse were enriched already in the DS-NPC specific clusters but not in the later appearing clusters specific for DS-imN and DS-GABA (**Figure 2F**). Additionally, the pathway of long-term potentiation, a hallmark for mature GABAergic cells, was specifically enriched in the DS-imN specific cluster but not in the DS-GABA clusters. Furthermore, representative annotated genes for Ctl- iPSC lines, PAX6 and GAD2 in the Ctl-NPC and Ctl-imN clusters, and GABRG3 in the Ctl- GABA cluster, exhibit a different tendency of chromatin accessibility in DS-iPSC clusters (**Figure 2G**), also shown by qPCR analysis (**Supplementary Figure 5E**). The enrichment of TF motifs and predicted pathways relevant for GABAergic interneuron appearing already in DS-NPC, but not in DS-GABA, uncovered a pattern distinct from that in Ctl-iPSC lines, that strongly suggest a perturbed GABAergic development associated with *SCN1A* variants.

Common chromatin dynamics in Ctl- and DS-iPSC models of GABAergic development

Identification of abnormal chromatin dynamics in GABAergic interneuronal development of DS-iPSC lines requires a thorough comparison with Ctl-iPSC lines. To extract shared dynamic chromatin features in DS-patient and Ctl-iPSC lines we first merged the differentially accessible chromatin peaks specific to each of the four time points (D0, D19, D35 and D65) within the Ctl and DS patient groups, respectively. The lists of all significant peaks in the Ctl- and DS- iPSC lines, respectively, were subsequently intersected to identify the common peak regions. In total, we identified 12,256 accessible chromatin peaks that show a shared and time-point specific pattern (**Figure 3A**, **Supplementary Table 5**).

Next, we sought to examine the genomic annotations, KEGG pathways, and TF motif enrichment for these common peaks (**Figure 3**). A K-mean clustering of read counts from the 12,252 accessible chromatin peaks revealed four common clusters (Com-1 with 6,264 peaks, Com-2 with 2,071 peaks, Com-3 with 1,793 peaks, and Com-4 with 2,124 peaks) (**Supplementary Figure 6**, **Figure 3A**). The DS-iPSC and Ctl-iPSC lines show a similar sequencing read count enrichment in Com-1 cluster and Com-2 clusters at the four time-points whereas slight differences are observed for the Com-3 and Com-4 clusters (**Figure 3A**). Accessible regions in Com-1 cluster are specifically open at D0 (iPSC) with annotations to TF genes for pluripotency such as *NANOG* and

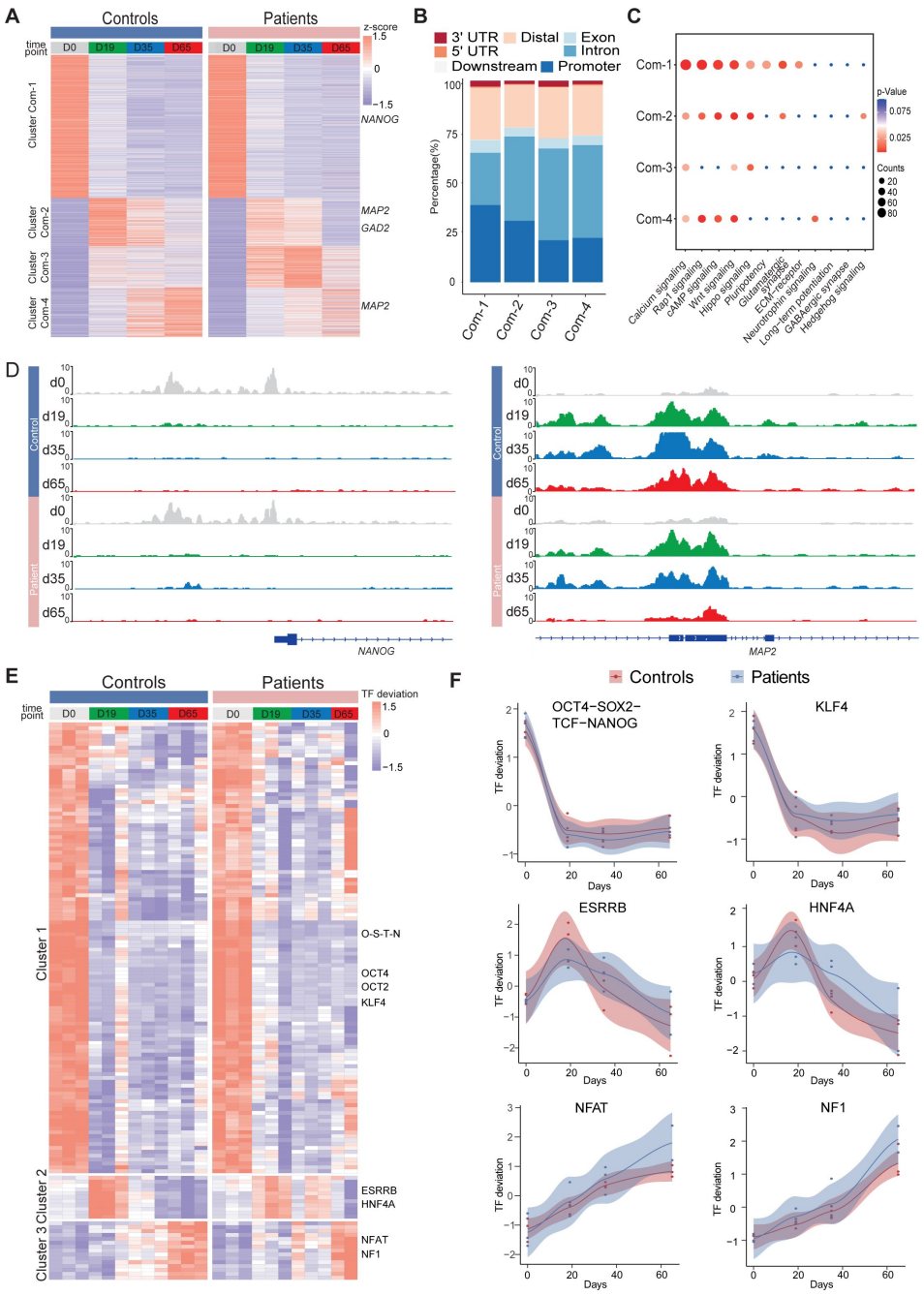

Figure 3

Common chromatin accessibility features of control and Dravet Syndrome patient iPSCs during GABAergic differentiation

A. Heatmap for common chromatin accessible regions detected between control and Dravet Syndrome (DS) group during differentiation. Four clusters were obtained from time series analysis. Representative genes are labeled on the right side of heatmap.

B. Barplot for genomic distribution of chromatin accessible regions for each cluster.

C. Bubble plot of KEGG pathway enrichment for each cluster. p-value and enrichment were indicated.

D. Genome browser view showing representative chromatin accessible regions at the indicated gene loci. These genes represent common changing regions between control and patients groups.

E. Transcription factors (TFs) deviation Z scores heatmap for unique TF enriched in each cluster. Representative TFs are labeled on the right side of heatmap.

F. Representative TFs enrichment (deviation Z score) dynamics at ATAC-Seq peaks in control and Dravet Syndrome (DS) group during differentiation.

SOX2, among others. The Com-1 cluster remains closed at the following three time-points. The Com-2 cluster is closed at D0 but open at D19 (NPC) with accessible peaks at genes such as *MAP2*, *NEUROD1*, and *NEUROG1*, among others (**Figure 3A**).

In both the Ctl and DS-patient groups, accessible regions in the Com-3 cluster are closed D0 but slightly open at D19 (NPC) and at D35 (imN) and then more closed at D65 (GABA). However, the degree of openness for a large proportion of peaks is much higher in the DS- patient group when compared to the Ctl group. Furthermore, at D65 (GABA) the Com-3 cluster shows accessible regions at NPC-specific genes such as *MAP2* and *ATOH1* but not for regulatory elements of GABAergic neuron-specific genes, such as *ASCL1*, *LHX6*, and *DLX2*, among others. The absence of common open chromatin regions at regulatory elements for GABAergic specific genes in the Ctl and DS-patient groups supports altered dynamics of accessible chromatin at the late time-point GABAergic development in our model system.

The genomic distribution of accessible peaks with respect to promoters, exons and introns varies between the Com-clusters (**Figure 3B**). The Com-1 cluster shows a relatively large proportion of accessible chromatin regions from promoter regions (38.2%) when compared to the other clusters (Com-2: 22.0%; Com-3: 20.8%, and Com-4: 30.5%). Conversely, the Com-1 cluster shows a relatively small proportion of accessible regions in intronic regions (25.8%) when compared to Com-2, 3 and 4 clusters. However, the genomic distribution of accessible peaks was very similar in the Com-2 and Com-3 clusters.

We then conducted KEGG analysis on genes within peaks of the four Com-clusters to understand the common biological features of the Ctl- and DS-iPSC lines. We observed enrichment for the pathways of transcriptional regulation of pluripotency, that included *NANOG*, in Com-1 (**Figure 3C**) and of nitric oxide-stimulated guanylate cyclase that included *MAP2* in Com-2 (**Figure 3D**). However, in the Com-3 or Com-4 clusters, characterized by an increasing open chromatin with development, we did not find enrichment in pathways relevant for GABAergic cells (**Figure 3D**). These observations further indicate similarities in the Ctl and DS iPSC-lines in cellular processes up to D19 (NPC), but significant differences at D35 (imN) and D65 (GABA).

Furthermore, we examined the enrichment of motifs for trans-acting transcription factors (TFs) from all common peaks and clustered TFs with a k-means method. The TF enrichment patterns are similar in the Ctl and DS groups, and three TF clusters were observed. Cluster 1, containing pluripotent-specific TFs such as OCT4 and KLF, among others, shows enrichment at iPSC in both the control and DS patient groups (**Figure 3E**, **3F**). Cluster 2, including TF motifs for the NPC-specific TFs ESRRB and HNF4A, is enriched in iPSC (D19) and imN (D35) (**Figure 3E**, **3F**), while some TFs relevant to GABAergic cells, such as NFAT and NF1, are enriched in D65. No GABAergic neuron-specific TFs (e.g., DLX, LHX, ASCL) are observed. Taken together, our data suggest similarities between Ctl- and DS-iPSC lines in accessible chromatin at loci for TFs important for GABAergic induction and early development. However, the Ctl- and DS- iPSC groups do not show similarities in the enrichment of TFs that are critical at later stages of GABAergic maturation.

Distinct chromatin features in DS-iPSC GABAergic development

A PCA analysis of ATAC-Seq data at D0 demonstrated that profiles of chromatin accessibility are similar in Ctl-iPSC and DS-iPSC-lines at d0 (iPSC) but different at d19 (NPC), d35 (imN), and d65 (GABA) (**Figure 4A**). These data suggest a diverging and disrupted trajectory of GABAergic development in our DS-iPSC model when compared to that in Ctl-iPSC.

To further understand the molecular regulators of dysfunctional GABAergic development in DS-iPSC, we extracted the chromatin accessible peaks that were mutually exclusive in the Ctl- and DS-iPSC lines at each time point (as described in the Methods section). The peaks were categorized into a Ctl distinct peak list and a DS distinct peak list. In total, the Ctl distinct peak list contained 3,311 accessible peaks (0 peaks at D0; 42 peaks at D19; 1,490 peaks at D35; and 1,779 peaks at D65),

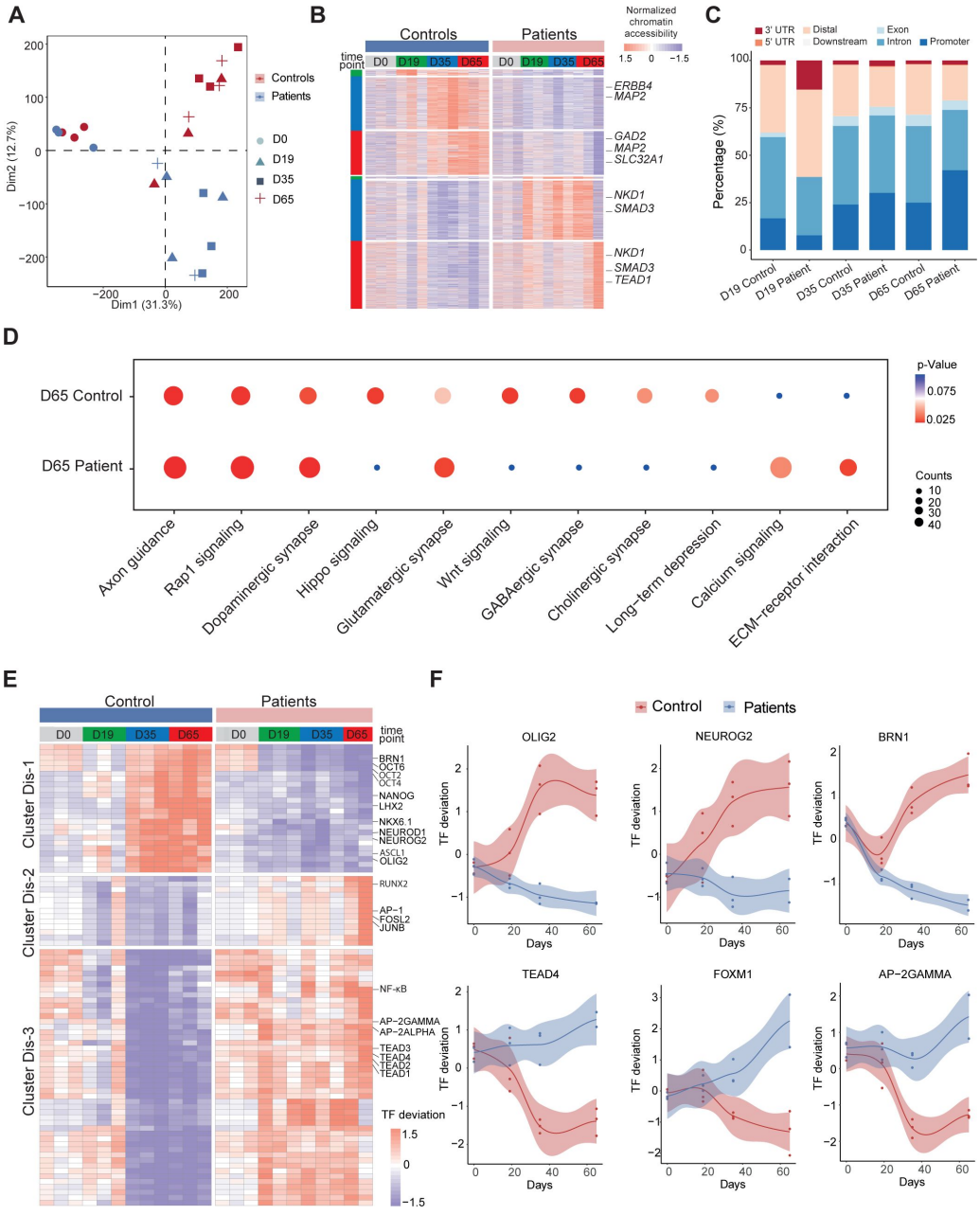

Figure 4

Unique chromatin accessibility features of control and Dravet Syndrome patient iPSCs during GABAergic differentiation

A. Principal component analysis (PCA) plot of all ATAC-Seq from control and Dravet Syndrome patients during GABAergic differentiation.

B. Heatmap showing the differential chromatin accessible peaks for comparison at each time point between the control and Dravet Syndrome (DS) patients. Representative genes are labeled on the right side of heatmap.

C. Barplot for genomic features of unique chromatin accessible regions at each time point for the control and Dravet Syndrome (DS) patients.

D. Bubble plot of KEGG pathway enrichment at GABAeric interneuron (Day 65) for the control and Dravet Syndrome (DS) patients. p-value and enrichment score were indicated.

E. Heatmap showing transcription factors (TFs) enrichment at differential chromatin accessible peaks for comparison at each time point between the control and Dravet Syndrome (DS) patients. Representative TFs are labeled on the right side of heatmap.

F. Representative TFs enrichment (deviation Z score) dynamics at ATAC-Seq peaks in control and Dravet Syndrome (DS) group during differentiation.

while the DS distinct peak list contained 4,434 accessible peaks (0 peaks at D0; 13 peaks D19; 1,708 peaks D35; and 2,713 peaks D65) (**Figure 4B**, **Supplementary** Figure 7A, **Supplementary Table 6**). These distinct peaks were located at different genomic regions (**Figure 4C**). Furthermore, KEGG enrichment analysis of the distinct peaks at D65 revealed pathways specific to cortical neurons, such as GABAergic synapse, Glutamatergic synapse, Dopaminergic synapse, and others, in Ctl-GABA but not in DS-GABA (**Figure 4D**, **Supplementary** Figure 7B,).

Next, we combined the distinct peak lists of the Ctl- and DS-iPSC lines and calculated enrichment of TF motifs using a systematic approach with chromVAR (chromatin variation across regions)[39]. We then performed a non-hierarchical clustering of TFs enriched in the distinct groups and identified three clusters (Dis-1, Dis-2, Dis-3) (**Figure 4E**). Cluster Dis-1 comprised two subclusters of TFs: Subcluster 1 included the OCT family of TFs (OCT2, OCT4, OCT6) and BRN1, with enrichment restricted to D0 (iPSC) in the DS group whereas in the Ctl group the enrichment was observed at D0, D35, and D65 but not at D19. Subcluster 2 included the GABAergic specific TFs OLIGO2, ASCL1, NEUROD1, NEUROG2, NKX6.1, LHX2, and others. These TFs were not enriched at any time-point in the DS group but enriched in the control group at D35 and D65 (**Figure 4F**). In cluster Dis-2, TFs such as JUNB, AP-1, RUNX2, and others were enriched in the DS group from d0 (iPSC) to D65 (GABA). However, in the Ctl group enrichment for Dis-2 cluster was observed only at D0 (iPSC). Cluster Dis-3 is enriched in both Ctl- and DS-iPSC for TFs of the TEAD family, AP-2 and NF-kappa beta. In the Ctl group, this enrichment increased significantly in NPC and decreased (disappeared) in imN and GABAergic neurons. Interestingly, the enrichment of these TFs in cluster Dis-1 persisted in the DS group with development from NPC to GABA. The absent enrichment of GABA -specific TF motifs at D65 in the DS group brings further support for a disrupted chromatin remodeling during interneuron development.

VPA induces changes in the chromatin landscape of iPSC derived GABAergic interneurons

Valproic acid (VPA) is a broad-spectrum anti-epileptic drug commonly used in the treatment of DS[1]. However, the response to VPA treatment varies considerable among affected individuals[40]. Prior reports suggest that the drug acts as a histone deacetylase (HDAC) inhibitor and thereby impacts chromatin remodeling[22,23]. We therefore hypothesized that chromatin changes induced by VPA in GABAergic cells may uncover processes contributing to therapeutic effects of the drug. To this end, we cultured Ctl- and DS-iPSC-derived GABAergic interneurons at D65 with and without VPA supplementation at therapeutic concentrations for six days. We then performed ATAC-Seq on three sample pairs of Ctl-GABA and on two pairs of DS-GABA (**Figure 5A**, **Supplementary** Figure 8A-D**, Supplementary Table 7)**. Subsequent PCA analysis of the ATAC-Seq data showed that VPA exposure induced variable changes in accessible chromatin that were seemingly iPSC-line specific (**Figure 5B**, **5C, Supplementary** Figure 8E). We then focused our analysis on the sample pairs showing the most extensive VPA-induced changes in chromatin accessibility, including two Ctl-GABA pairs (Ctl1B and Ctl7C) and one DS-GABA pair (DD5A; **Figure 5C**). Genomic annotation revealed that chromatin changes induced by VPA were distributed in promoters, introns, and distal regulatory elements and at a variable extent when comparing individual Ctl and DS pairs (**Supplementary Figure 8F**). The regions showing VPA induced changes in accessible chromatin were distributed in promoters, introns, and distal regulatory elements (**Figure 5D**). The changes in chromatin accessibility after VPA treatment observed in both the Ctl- and DS- GABA may reflect unspecific effects of the drug. To validate our hypothesis on chromatin specific effects of VPA we performed enrichment analysis of differentially accessible peaks for each iPSC-GABA pair. The results show enrichment in chromatin-relevant pathways in both Ctl and DS pairs (**Figure 5E**). The analysis of open chromatin in response to VPA in Ctl- and DS-GABA thus suggest drug-induced changes that are unspecific and genome-wide. This is in line with the reported unpredictable effects of VPA on seizure frequencies in DS.

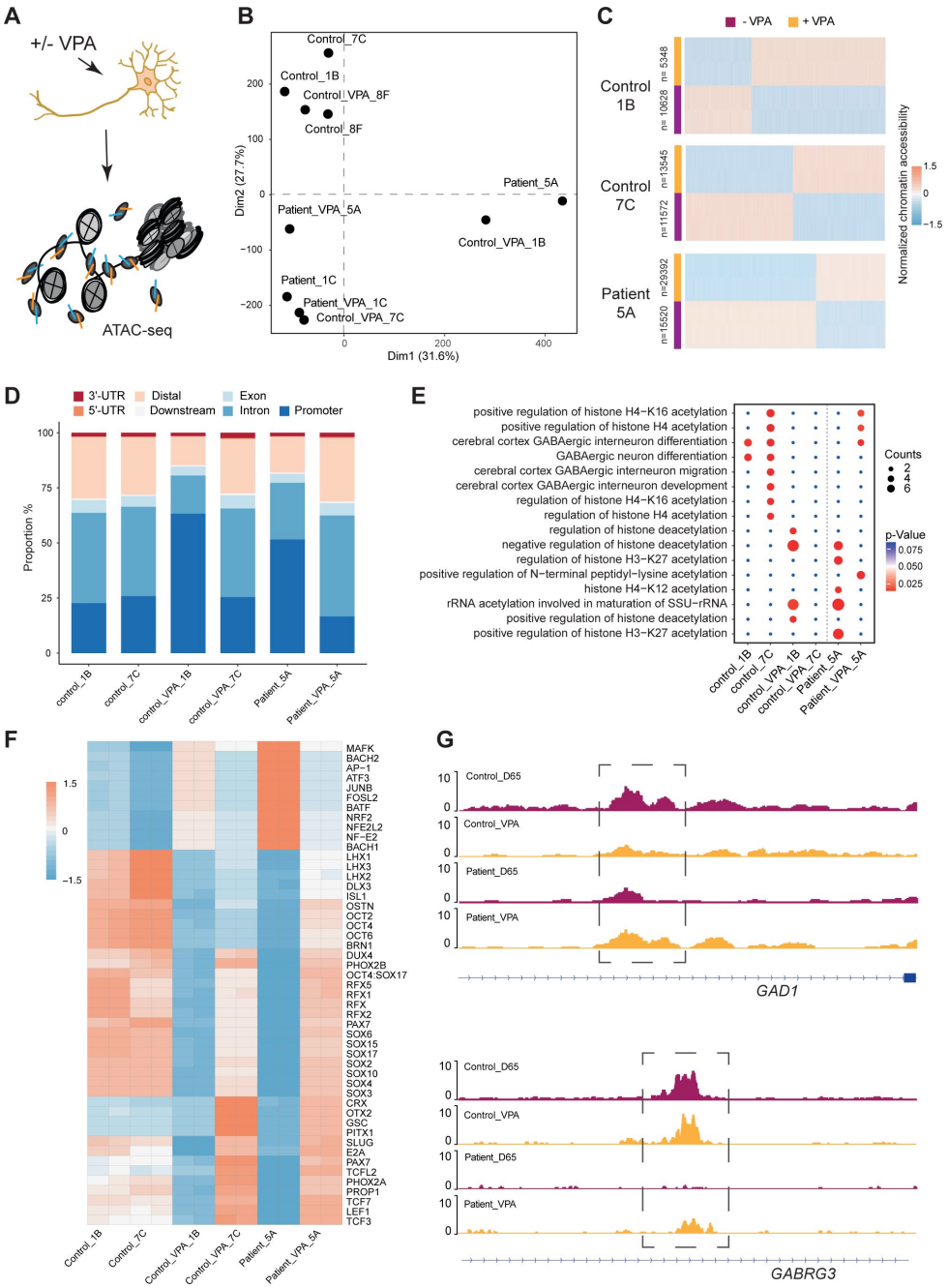

Figure 5

Chromatin accessibility response to Valproic acid treatment in GABAergic interneurons

A. Schematic illustration showing measurement of chromatin accessibility response in valproic acid (VPA) treatment of GABAergic interneurons.

B. Principal component analysis (PCA) plot of ATAC-Seq with and without VPA treatment of GABAergic interneuron in control and Dravet Syndrome patients.

C. Heatmap of differential chromatin accessible peaks from the VPA responsible group, consisting of two control samples and one Dravet Syndrome (DS) patient sample.

D. Barplot for genomic distribution of VPA responsible accessible regions from differential conditions.

E. Bubble plot of KEGG pathway enrichment for each condition. p-value and enrichment were indicated.

F. TF deviation Z score heatmap for top 50 transcription factors (TFs) enriched at responsible chromatin regions from differential conditions.

G. Genome browser view showing representative VPA responsible chromatin accessible regions at the indicated gene loci.

Since VPA treatment has an effect on seizure frequencies in a subgroup of affected individuals, we investigated whether VPA could "restore" the chromatin accessibility profile of DS-GABA into the chromatin profile of Ctl-GABA. The pathways relevant for GABAergic cells became enriched in the chromatin regions that become accessible after VPA treatment in the DS-GABA sample pair (**Figure 5E**). A specific analysis of TF motifs becoming accessible in VPA-treated DS-GABA uncovered enriched motifs for TFs relevant for GABAergic development, such as LHX3, SOX and the RFX families of TFs (**Figure 5F**). Conversely, Ctl-GABA pairs showed an opposite enrichment pattern for these TF motifs upon VPA treatment. Furthermore, both Ctl- and DS-GABA showed a VPA-induced increase in chromatin accessibility at regulatory regions of GABAergic specific genes, such as GAD1 and GABRG3 (**Figure 5G**). Taken together, our iPSC model suggests that VPA has the potential to dramatically interfere with and change chromatin structure in GABAergic cells. These changes are likely unspecific and may affect genes important for interneuronal development.

Discussion

The majority of cases with DS are pharmaco-resistant and there is an urgent need to improve our understanding of the underlying mechanisms for the development of targeted anti-seizure treatments [2,40,41]. To this end, we used our iPSC-based model of GABAergic development in DS caused by heterozygous *SCN1A* variants. The model system recapitulates hallmarks of the disease and we therefore reasoned that it may improve our knowledge on DS-associated epigenetic changes as well as chromatin modifications induced by the commonly used anti-seizure drug VPA[13,29]. Specifically, we differentiated iPSCs from healthy donors (Ctl) and DS-cases towards GABAergic cortical interneurons and characterized the dynamic chromatin conformational changes using ATAC-Seq. To our knowledge, this is the first study that describes chromatin accessibility changes in DS-patient derived iPSC neurodifferentiation. We identified common and distinct chromatin accessibility profiles when comparing iPSC of DS patients and healthy donors at different time points of GABAergic development. As expected, the chromatin profiles of undifferentiated iPSC are similar in the two groups, with accessible peaks for TF genes maintaining a pluripotent state, such as *NANOG* and *POU5F1*. Differentiation towards a GABAergic fate shows that both Ctl and DS iPSC-lines acquire accessible chromatin peaks associated with genes enriched in pathways relevant for interneuronal development (e.g. signaling pathways, GABAergic synapse and long-term potentiation). However, our analyses uncovered increased changes in accessible peaks at the early phase (D19) of GABAergic development in DS-patient cells when compared to the control group. At the same time-point (D19) we also detected expression of *SCN1A*, providing a link between altered sodium flux and aberrant chromatin dynamics in DS-iPSC derived neurons. The genes associated with the distinct temporal changes of open chromatin in DS- patient cells are enriched in KEGG terms such as GABAergic synapse, Glutamatergic synapse and Long-term potentiation, suggesting a perturbed and seemingly accelerated initial GABAergic induction before D35. The enrichment in these pathways is lost with further differentiation of DS derived iPSC-lines and they fail to acquire the chromatin profile of Ctl GABAergic cells at D65. The aberrant chromatin profiles in our iPSC model comply with previous studies on iPSC and mice models of DS showing both transcriptional and electrophysiological changes in interneurons[9,13,42]. In our prior study, the transcriptional changes emerged predominantly after D19, the ATAC-Seq analysis in the current study show alterations in chromatin structure already at D19. This observation confirms that epigenetic changes detected by ATAC-Seq precede the transcriptional changes[30]. Furthermore, our study defines differential accessible chromatin regions and TF motifs associated with heterozygous and pathogenic *SCN1A* variants, bringing further insights into disturbed interneuronal differentiation in DS. In control iPSC lines, the chromatin accessibility of motifs for TFs relevant to drive neurogenesis, such as NEUROG2, OLIG2, BRN1, increase with differentiation whereas the same regions are closing in DS derived iPSC. On the other hand, motifs of more general TFs, such as TEAD4, FOXM1, AP-2GAMMA, become either accessible or un-accessible with differentiation in control iPSC but remain closed or open in differentiating DS iPSC. This is consistent with our previous observations in DS-GABA showing

dysregulated expression of *FOXM1* and of genes enriched in pathways for histone modification and cell cycle pathways[13]. Moreover, similar to the *Scn1a* +/- mice model, showing an intact density of cortical and hippocampal GABAergic interneurons despite impaired functions[20], our immunostainings revealed a comparable number and morphology of DS-patient and Ctl GABAergic neurons. These observations suggest that the proliferative capacity is relatively preserved during GABAergic interneuron development in DS.

Currently, valproic acid (VPA) is commonly used as one of the first line drugs in DS[1] but the response on seizure frequencies is highly variable among affected cases[43,44]. The mode of action of VPA is not fully understood but it is believed to inhibit histone deacetylases, leading to changes in chromatin states and gene expression[25,45]. In our study, we aimed to study the epigenetic effect of VPA administration on iPSC derived GABAergic neurons derived from DS patients and healthy donors. The GABAergic interneurons exposed to therapeutic concentrations of VPA for six days showed extensive changes in accessible chromatin peaks in our cultures. Projection of the chromatin changes using KEGG uncovered pathways that reflect the expected mode of action of VPA, such as *histone acetylation* and *deacetylation* and *rRNA acetylation*, of importance for transcriptional activity.

However, the VPA-induced chromatin modifications in iPSC-GABA varied considerably with biological origin and the accessibility changes linked to GABAergic development were specific or shared for individual iPSC-GABA-lines. For example, in Ctl-GABA we observe an enrichment for LHX1-3 and DLX3 motifs that changes from open to closed after VPA exposure. In contrast, DS-GABA show a somewhat opposite enrichment pattern for LHX and DLX binding motifs after VPA exposure that changes from closed to open. In mice, motifs for the LHX and DLX family of TFs are enriched in the late interneuronal development that extends postnatally[19]. In addition, Ctl-GABA show a reduction in accessible SOX-binding motifs after VPA treatment whereas DS-GABA show an opposite response, acquiring a profile more similar to the untreated Ctl-GABA. The SOX-family of TFs has a global impact on both embryonic and adult neurogenesis[46] and enrichment of SOX binding motifs are enriched in migratory interneurons[19]. These observations may suggest a mechanism by which VPA, at least in some cases, facilitates accessibility for TFs with beneficial effects on postnatal GABAergic function. Moreover, VPA treated DS-GABA uncovered enriched changes for TF motifs for AP-1 and BRN1 that made the cells acquire a pattern more similar to that in control lines. It may therefore be hypothesized that VPA induces unspecific changes in chromatin structure of iPSC-GABA that, at least in some cases, may lead to an increased accessibility for TFs linked to GABAergic development. Such a variability in response to VPA exposure in our model is consistent with the unpredictable effects of VPA on seizure-frequencies, even in cases with identical *SCN1A* variants[40], mediated by epigenetic factors that are specific to individuals. Finally, our iPSC model of GABAergic development has limitations that should be considered. The model system applies a directed protocol during 65d that may not fully recapitulate maturation of GABAergic cells *in vivo*. Functional maturation of GABAergic interneurons occurs postnatally in humans, and models using direct differentiation from iPSC typically do not reach into cellular states comparable to postnatal cell types. More complex neuronal systems, such as 3D organoids from isogenic iPSC lines and in long-term cultures, in combination with single cell analysis, will be needed to confirm our data. Nevertheless, our findings represent an important step forward to clarify epigenetic changes in inhibitory interneurons that are associated with the progression to DS, adding data to a frame-work of knowledge for the development of targeted and personalized therapies. Further studies are now required to increase the number of independent iPSC lines with pathogenic *SCN1A* variants to validate our findings on epigenetic changes in DS and the effects of anti-seizure drugs such as VPA.

Materials and Methods

Cell culture, GABAergic differentiation and sampling

iPSC lines from three patients (DD1C, DD4A, DD5A)[29] and three controls (Ctl1B, Ctl7C, Ctl8F)[47] were cultured on human recombinant laminin LN521 (Biolamina) in Essential-8™ medium (Thermo Fisher Scientific) and passaged using Trypl Express (Thermo Fisher Scientific) as described[29]. GABAergic interneuron differentiation from iPSCs was performed as previously described[13]. The protocol utilizes DUAL SMAD inhibition to induce neurogenesis towards neural stem cells for 10 days, followed by patterning with high levels of sonic hedgehog for nine days towards cortically fated neuronal progenitor cells (NPC) that mature for 46 days, i.e. a total of 65 days (**Figure 1A**). Neuronal cells at day 65 and onwards are viable as judged by morphological assessment by light microscopy. Differentiation was repeated at least three times per cell line.

Cell cultures were sampled at days 0 (D0), D19, D35 and D65, respectively, by harvesting cells with TryplE and collecting by centrifugation (300 x g, 3 min). Harvested cells were counted and assessed for viability using trypan blue staining and an automated EVE cell counter (NanoEntek). Samples with a viability of >90% were selected for ATAC-Seq library preparation (see below). Additionally, neuronal cell cultures at D65 were treated with valproic acid (VPA; 0,5 mM) for 6 days and subsequently harvested for analysis. Harvested cells were resuspended in 1 ml of 1 x PBS and fixed by adding an equal amount of 2% formaldehyde for 10 min at room temperature. The reaction was quenched by adding 100 ul 2,5 M glycine solution. Fixed cells were collected by centrifugation and washed twice with 1 x PBS. Cells where then resuspended in 1 x PBS, counted using an EVE automatic cell counter (NanoEntek) with Trypan Blue, and subsequently 50’000 cells/sample were processed for library preparation for ATAC sequencing.

Tn5 transposome assembly

Tn5 transposome assembly was performed by as previously described[48]. Briefly, 2 µM annealed Tn5MErev/Tn5ME-A, 2 µM annealed Tn5MErev/Tn5ME-B, and 2 µM Tn5 transposase (Protein Science Facility at Karolinska Institutet, Stockholm) in dialysis buffer (50 mM HEPES-KOH at pH 7.2, 50 mM NaCl, 0.05 mM EDTA, 0,5 mM DTT, 0.05% Triton X-100, 5% glycerol) with 40% glycerol were mixed, incubated for 1 h at room temperature and subsequently stored at −20°C until use. The adaptor oligonucleotides (Tn5MErev: 5’-/Phos/CTGTCTCTTATACACATCT-3’, Tn5ME-A: 5' -TCGTCGGCAGCGTCAGATGTGTATAAGAGACAG-3' and Tn5ME-B: 5'-GTCTCGTGGGCTCGGAGATGTGTATAAGAGACAG-3') were synthesized by Integrated DNA Technology. For oligo annealing, equimolar amounts of Tn5MErev and Tn5ME-A or Tn5ME-B and Tn5MErev, respectively, were combined in a PCR tube and annealed using the following program: 95°C for 5 min, ramp down to 25°C with −0.1°C/s increments.

ATAC-Seq library preparation and sequencing

ATAC-Seq libraries were prepared following[48]. In brief, two technical replicates per sample containing 50,000 nuclei each were collected at 500 x g for 5 min at 4°C. Nuclei were resuspended in lysis buffer (10 mM Tris-Cl, pH 7.4; 10 mM NaCl; 3 mM MgCl2; 0.1% Igepal CA-630) and centrifuged at 500 x g for 10 min. The supernatant was removed and each nuclei pellet was resuspended in tagmentation buffer (25 µL 2 × TD buffer) with 2.5 µl Tn5 transposome and incubated at 37°C for 30 min. An equal volume of 2 x reverse crosslinking buffer (50 mM Tris-Cl, 1mM EDTA, 1% SDS, 0.2M NaCl, 5 ng/ml Proteinase K) was added to each sample and incubated at 65°C with agitation at 1200 rpm for overnight. DNA was isolated using a MinElute PCR Purification Kit (Qiagen). Sequencing libraries were prepared following described standard protocol[49]. All libraries were sequenced on an Illumina Nova-seq platform at Novogene Europe.

RNA isolation and quantitative RT-PCR

Total RNA from iPSCs and differentiated cell populations was isolated using a miRNeasy micro kit (Qiagen). 1 µg of total RNA was reverse transcribed into cDNA using High Capacity cDNA transcription kit (ThermoFisher Scientific). Expression of marker genes was compared to expression of the two housekeeping genes GAPDH and ACTB. FastStart Universal SYBR Green Master mix (Roche) was used for qPCR using the following primers: ACTB-For: CAGGAGGAGCAATGATCTTGATCT; ACTB-Rev, TCATGAAGTGTGACGTGGACATC; GAPDH-For, GAAGGTGAAGGTCGGAGTC; GAPDH-Rev, GAAGATGGTGATGGGATTTC; SCN1A-For, TGAAGAATCCAGGCAGAAATGC; SCN1A-Rev, TCGAAATGAACGGAGAACAGA; NANOG-For, CAGCCCCGATTCTCCACCAGTCCC; NANOG-Rev, CGGAAGATTCCCAGTCGGGTTCACC; PAX6-For, AACAGACACAGCCCTCACAAACA; PAX6-Rev, CGGGAACTTGAACTGGAACTGAC; GAD2-For, AGCTGCAGCCTTAGGGATTG; GAD2-Rev, TTGCAAATGTCAGCGACAGC; GABRG3-For, TCATGGGCCTCAGAAACACC; GABRG3-Rev, CTTGCTGGCGTAGCATCTTTT. For all analyses, we used samples from three independent differentiation cultures and each sample was analyzed in triplicate. Expression was calculated as ΔCT(gene X, day Y) = CT(gene X, day Y) - CT(AVERAGE (GAPDH/ACTB, day Y)) and fold change was calculated as ΔΔCT(gene X, day Y) = ΔCT(gene X, day Y) - ΔCT(gene X, day 0) and presented as log2 [2^-(ΔΔCT)] ±SD.

Immunofluorescence staining

Staining was performed on cells fixed with ice-cold 4% PFA and subsequently permeabilized in blocking solution (1 x PBS pH 7.4, 1% BSA, 0.1% Triton X-100). Primary antibodies against MAP2 (1:5'000; abcam, Cambridge, United Kingdom), GABA (1:1'000; Sigma, MO, United States), GAD1 (1:100, Millipore, MA, United States) and DCX (1:100, Santa Cruz, United States) were used for immunostaining and quantification. Primary antibodies were allowed to bind overnight separately or in appropriate combinations at 4°C. After washing three times in 1 x PBS, the secondary antibodies donkey anti-goat IgG AlexaFluor 633, donkey anti-rabbit IgG AlexaFluor 568 or donkey anti-mouse IgG AlexaFluor 488 (1:1'000; ThermoFisher Scientific, Waltham, MA, United States) were applied alone or in appropriate combinations for 1.5 h at room temperature in the dark. Visualization was performed on a Zeiss 510 confocal microscope (Carl Zeiss Microscopy, Jena, Germany) using Zen 2009 imaging software. Image processing was carried out using FIJI software.

Bioinformatic and statistical analyses

ATAC-Seq data processing and quality analysis

After the Adapter sequence trimming, the ATAC-Seq sequencing reads were mapped to genome hg38 using bowtie2[50]. Mapped paired reads were corrected for the Tn5 cleavage position by shifting +4/-5 bp depending on the read strand. All mapped reads were extended to 50 bp centered around the Tn5 offset. PCR duplicates were removed using Picard (*http://broadinstitute.github.io /picard/*), and sequencing reads from chromosome M were filtered out. The Peak calling of each ATAC-Seq library was performed with MACS2[51] with parameters -f BED, -g hs, -q 0.01, --nomodel, --shift 0. Peaks were merged into a matrix using bedtools merge [52]. Raw reads within peaks were normalized using EdgeR's cpm function [53]. Log transformation was applied to these normalized peaks to calculate the Pearson correlation among duplicates. Differential ATAC peaks for clusters were selected using DESeq2[54] with the following cutoffs: false discovery rate (FDR) < 0.05, |log2 fold change| > 1, and peak average intensity > 16. FDR values are Benjamini-Hochberg procedure corrected per default settings.

Chromatin accessibility dynamic across differentiation

To avoid capturing the dynamic changes of accessible regions caused by variability across individuals, we initially compared the dynamic changes of chromatin accessibility cell line by cell line across differentiation. Subsequently, we extracted the common changes observed across different cell lines at each time point. Cluster analysis was conducted on both control and patient groups of ATAC-Seq data at different time points during differentiation (D0, D19, D35, and D65). The raw data were processed with background correction and normalization using Reads Per Kilobase per Million mapped reads (RPKM). Clustering analysis was performed separately for the control and patient groups of ATAC-Seq data using the Mfuzz package[55], with minimum standard deviation and Z score parameters set at 1 and 0.5, respectively. Clusters were assigned based on the chromatin accessibility patterns of differential chromatin accessible peaks. Subsequently, clusters exhibiting significant changes were selected for further analysis.

Annotation of unique ATAC peaks to genes and KEGG pathway analysis

Genomic annotation of each ATAC-Seq peak to its nearest gene for the differential accessible regions was done using ChIPseeker[56]. A gene promoter region was defined as 3 kb upstream and 3 kb downstream of the transcription start site. The peaks were annotated to their nearest gene within a 10 kb distance from the transcription start site (TSS). Subsequently, Clusterprofiler[57] was used to perform Kyoto Encyclopedia of Genes and Genomes (KEGG) pathway enrichment analysis, and the results were ranked by false discovery rate (FDR). An FDR of less than 0.05 was set as significant.

Transcription factors (TFs) motif enrichment analysis

TF motif enrichment was performed with HOMER [58] using the differential accessible regions as input. For TF binding prediction, chromVAR [39] was employed. In brief, the Homer vertebrate TF database was used as input for TF motifs in chromVAR, and then TF accessibility deviation values were calculated for each sample across the entire sample set. TF deviations with a threshold greater than 2 were retained, and TF motifs with a positive correlation with one group/cluster were selected to represent that group/cluster. TFs were ranked based on their variability within each group/cluster, and z-scores of deviations from each TF were visualized in a heatmap.

Author contributions

Conceptualization: JS, ND, XC; Methodology: JS, XL, YD, JK, AW; Analysis and Investigation: JS, XL, YD, JK, ND, XC; Data curation and Visualization: JS, XL, YD, JK; Writing – original draft: JS, XC; Writing – Review and Editing: JS, XL, JK, YD, ND, XC; Supervision: ND, XC; Funding Acquisition: ND, XC.

Declaration of interest

The authors declare that no conflicting interest exists.

Acknowledgements

Research in the lab is funded by the Swedish Research Council (2020-01947 to N.D. and 2022- 00658 to X.C.), Hjärnfonden (FO2020-0171 and FO2022-0042 to ND), Swedish Cancer Foundation (21 1449Pj, 22 0491 JIA to X.C.), Stiftelsen Margarethahemmet (to N.D.) and Sävstaholm Society (to J.S.), Wallenberg Academy Fellow from Knut and Alice Wallenberg foundation (2023.0046 to X.C.), Uppsala University and Science for Life Laboratory. The funders played no role in study design, data acquisition and interpretation or decision to publish.

Availability of the data

The ATAC-Seq data generated for this study have been deposited in the Sequence Read Archive (SRA) with the following number: PRJNA1013337.

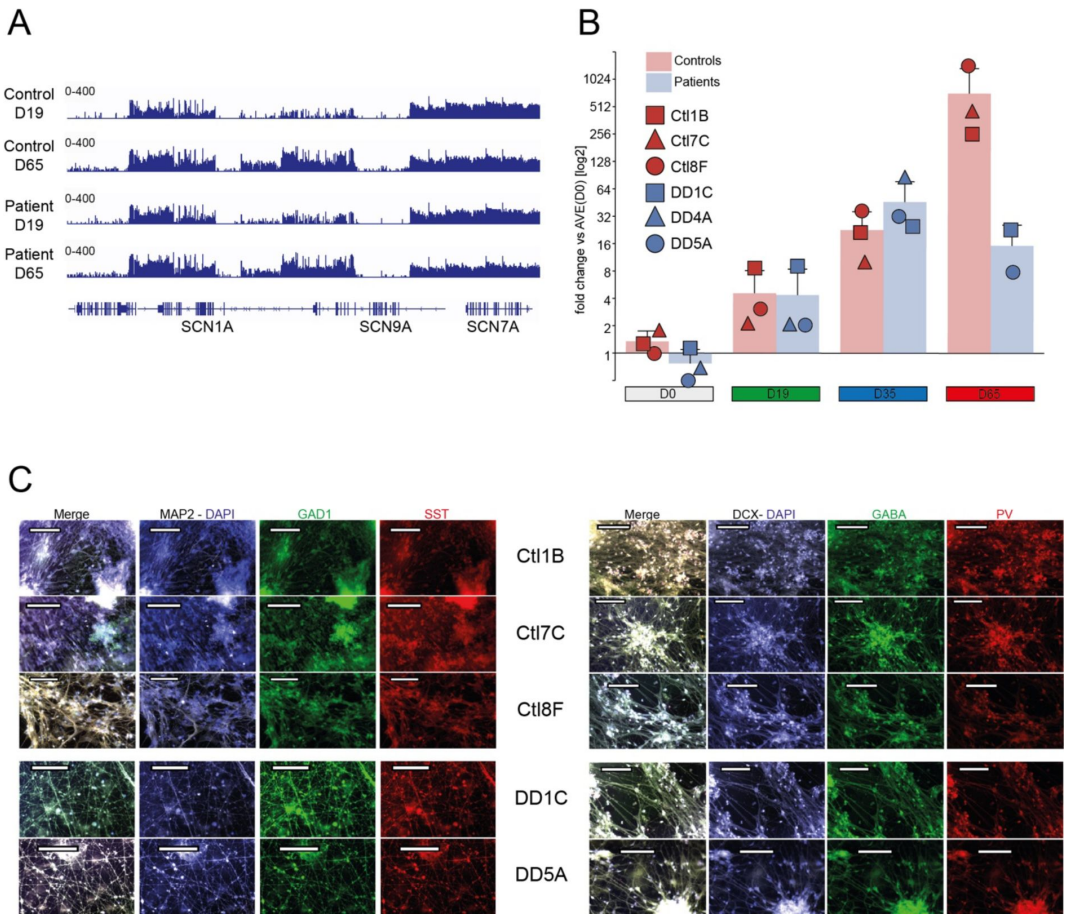

Supplementary Figure 1

validation of GABAergic differentiation.

A. *SCN1A* gene expression at day 19 and day 65 from RNAseq.

B. *SCN1A* expression levels quantified by qRT-PCR following GABAergic differentiation of control and patient iPSC relative to expression of the housekeeping genes ACTB and GAPDH at D0, D19, D35 and D65. Fold change data are presented as log2 [mean ΔΔCT(day Y)] ± SD and individual data points for each cell line are indicated (Control lines in red: Ctl1B - square, Ctl7C - triangle, Ctl8F – circle; patient lines in blue: DD1C - square, DD4A - triangle, DD5A – circle; please see Methods for detail). Ctl1B, Ctl7C, Ctl8F, DD1C, DD4A, DD5A are names of cell lines.

C. Representative pictures of immunofluorescent staining of Ctl-iPSC and DS-iPSC derived GABAergic neurons at D65 (Ctl-GABA) of GABAergic interneuron differentiation. The GABA cells form networks and stain positive for the neuronal markers MAP2 and double cortin (DCX), the GABAergic marker γ- aminobutyric acid (GABA) and the interneuronal markers somatostatin (SST), parvalbumin (PV) and glutamate decarboxylase 1 (GAD1). Size bar 100 µm.

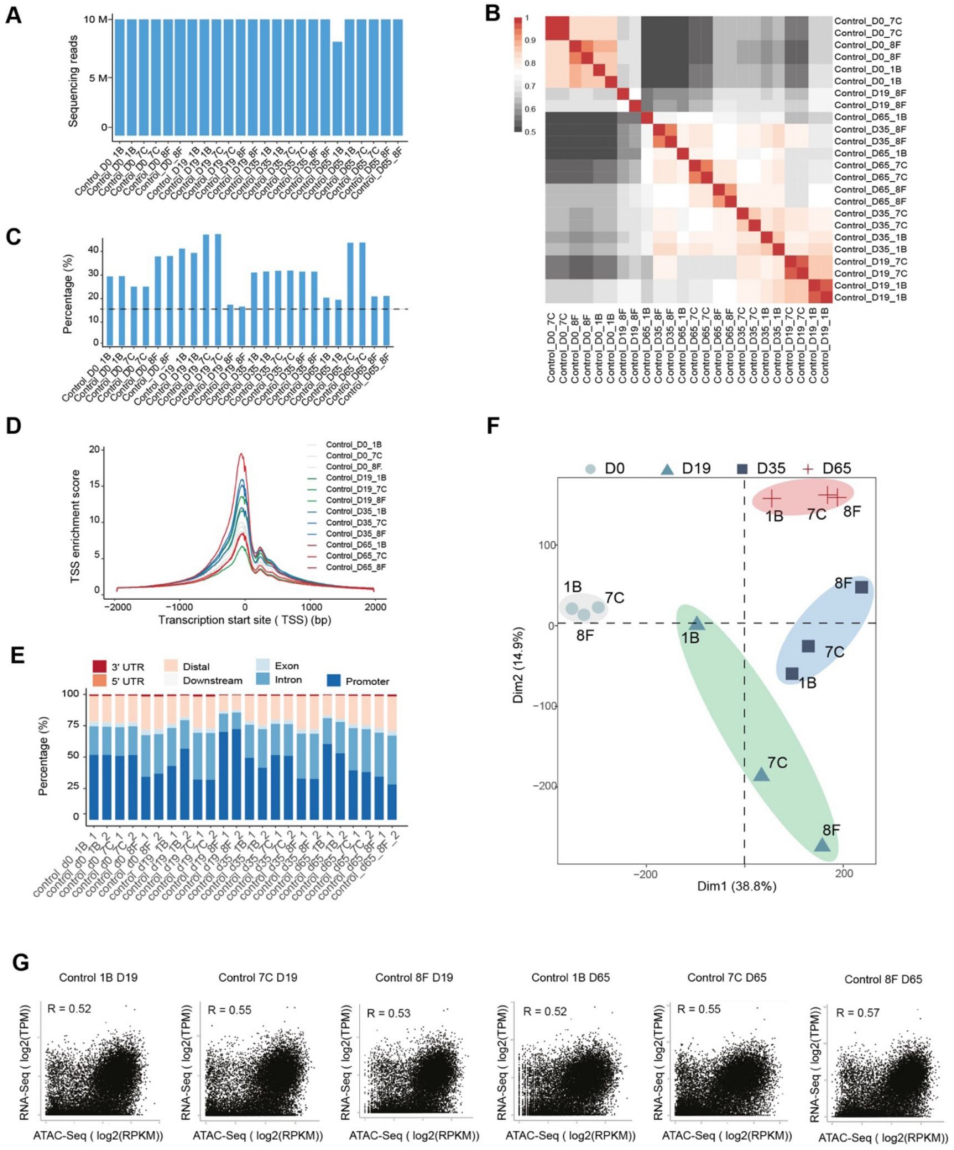

Supplementary Figure 2

Quality control of ATAC-Seq samples during GABAergic interneuron differentiation of Ctl-iPSC.

A. Sequencing depth for each sample.

B. Pearson correlation matrix from technical duplicates of ATAC-Seq at different time points.

C. Quantification of fraction of reads in peaks (FRiP) of ATAC-Seq in each condition. The dotted line indicates the cutoff used.

D. Transcription start site (TSS) enrichment score of ATAC-Seq in each sample.

E. Genomic distribution of chromatin accessible peaks for each sample.

F. Principal component analysis of ATAC-Seq from each sample.

G. Pearson correlation of gene expression from RNA-Seq and chromatin accessibility from ATAC-Seq.

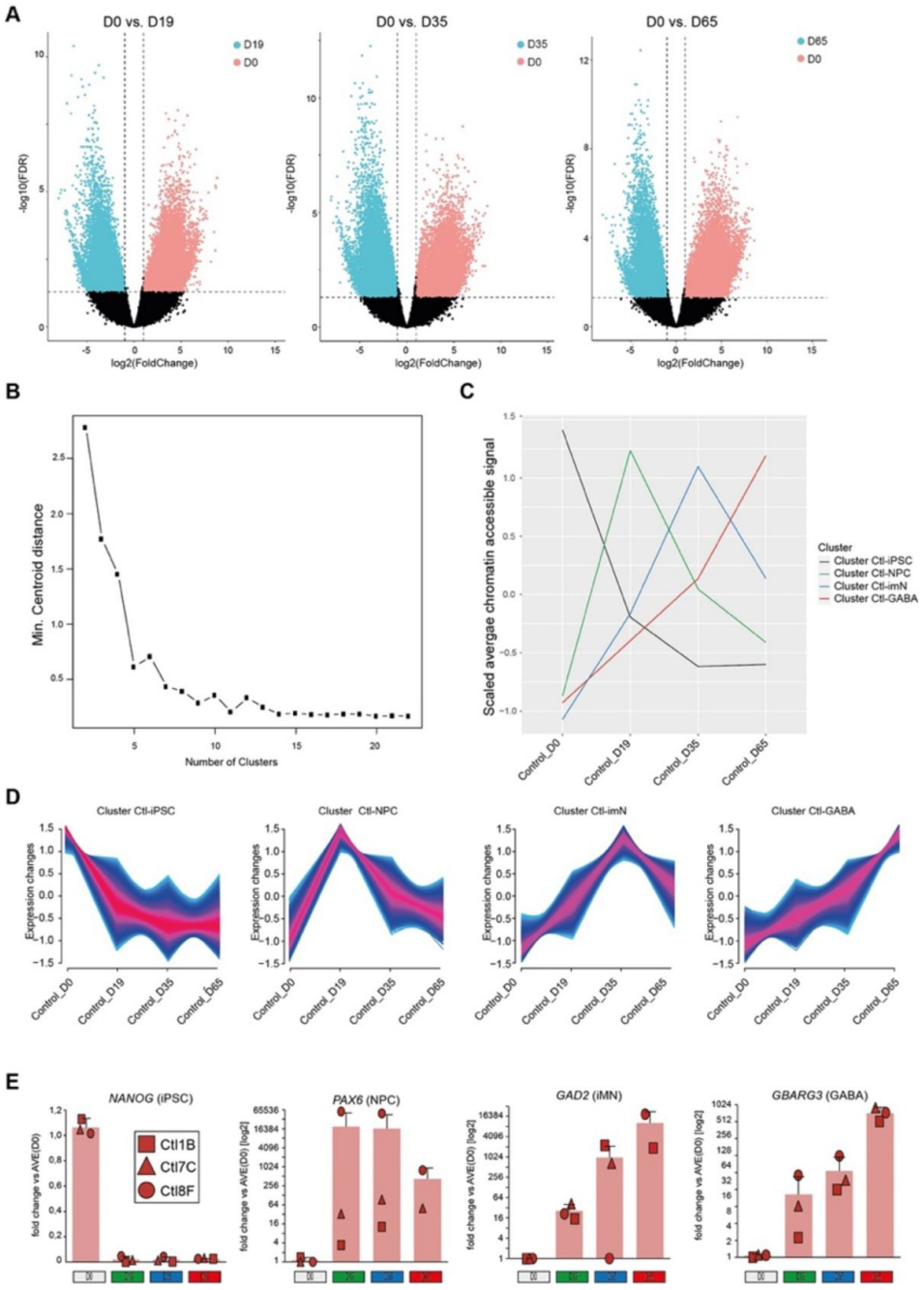

Supplementary Figure 3

Chromatin accessibility cluster identification during GABAergic interneuron differentiation of Ctl-iPSC.

A. Volcano plots show differential accessible chromatin peaks between D0 and different time points. D0 (n = 6046) vs. D19 (n = 3866); D0 (n = 8880) vs. D35 (n = 7865); D0 (n = 7870) vs. D65 (n = 7776). The dotted lines indicate the cutoff used to identify differential ATAC-Seq peaks.

B. Variance with different numbers of clusters derived from chromatin accessibility during GABAergic interneuron differentiation

C. The scaled average chromatin accessibility during GABAergic interneuron differentiation from each cluster.

D. The tendency of chromatin accessibility during GABAergic interneuron differentiation from each cluster.

E. Expression of the four cluster markers *NANOG* (iPSC; D0), *PAX6* (PNC; D19), *GAD2* (imN; D35) and *BABRG3* (GABA; D65) quantified by qRT-PCR following GABAergic differentiation of control iPSC relative to expression of the housekeeping genes ACTB and GAPDH. Fold change data are presented as log2 [mean ΔΔCT(day Y)] ± SD and individual data points for each cell line are indicated (Control lines in red: Ctl1B - square, Ctl7C - triangle, Ctl8F – circle please see Methods for detail).

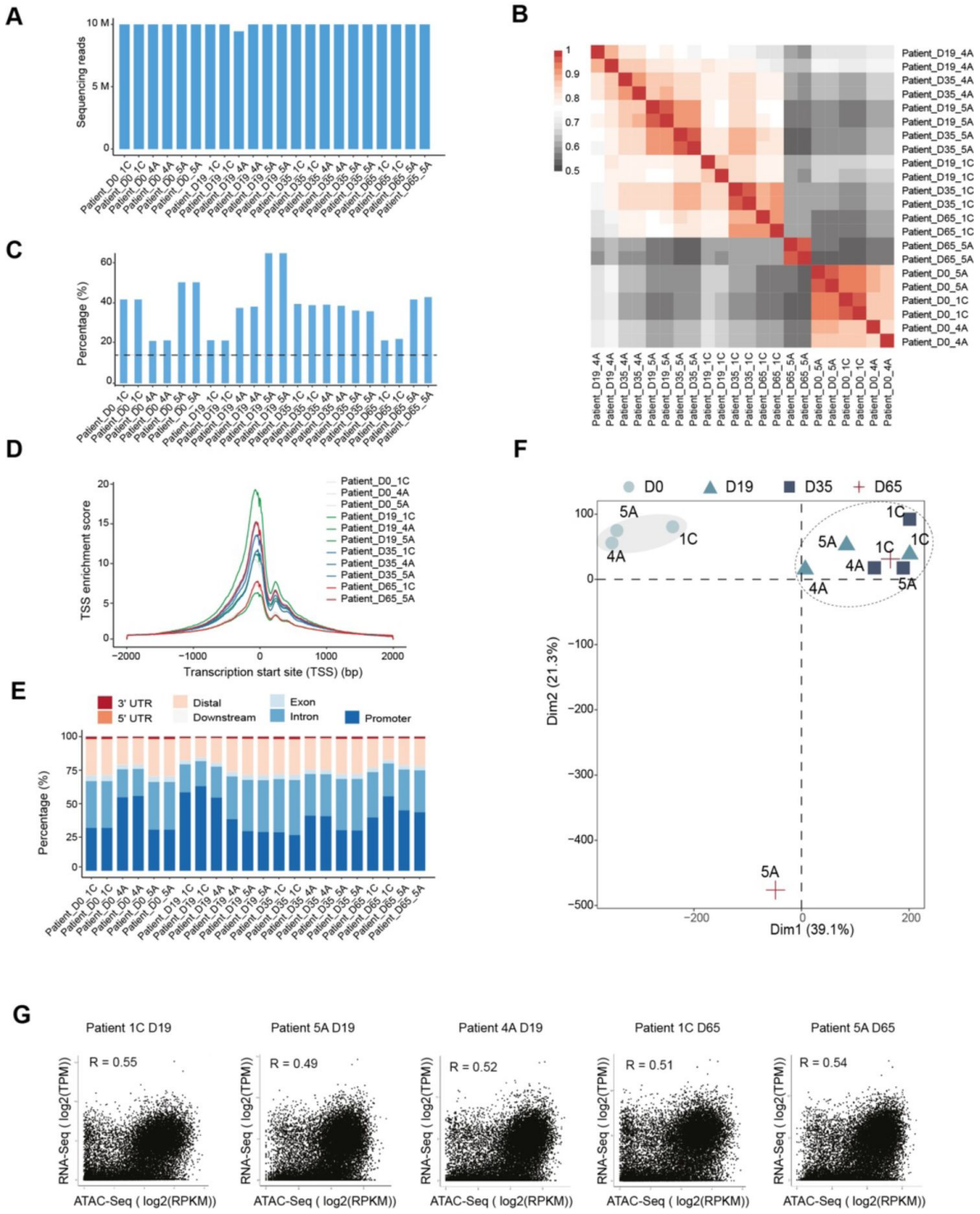

Supplementary Figure 4

Quality control of ATAC-Seq samples during GABAergic interneuron differentiation in Dravet Syndrome patient iPSCs.

A. Sequencing depth comparison from each sample.

B. Pearson correlation matrix from technical duplicates of ATAC-Seq from all samples.

C. Quantification of fraction of reads in peaks (FRiP) of ATAC-Seq in each condition. The dotted line indicates the cutoff was used.

D. Transcription start site (TSS) enrichment score of ATAC-Seq in each sample.

E. Genomic distribution of chromatin accessible regions for each sample.

F. Principal component analysis of ATAC-Seq from each sample.

G. Pearson correlation of gene expression from RNA-Seq and chromatin accessibility from ATAC-Seq.

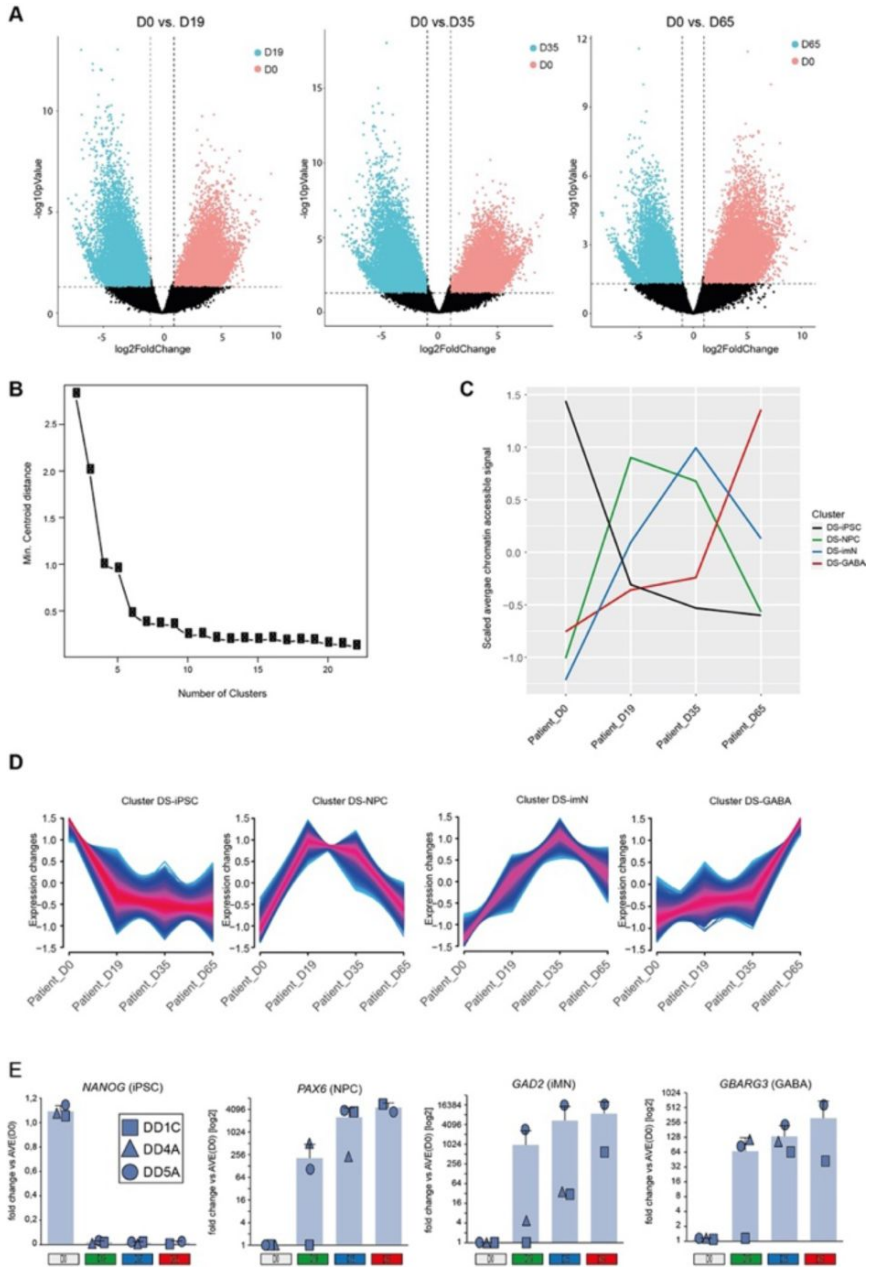

Supplementary Figure 5

Chromatin accessibility cluster identification during GABAergic interneuron differentiation in Dravet Syndrome patient iPSCs.
A. Volcano plots show differential accessible chromatin peaks between D0 and different time points. D0 (n = 7798) vs. D19 (n = 5183); D0 (n = 10154) vs. D35 (n = 7239); D0 (n = 6909) vs. D65 (n = 5667). The dotted lines indicate the cutoff used to identify differential ATAC-Seq peaks.
B. Variance with different numbers of clusters derived from chromatin accessibility during GABAergic interneuron differentiation in Dravet Syndrome patients.
C. The scaled average chromatin accessibility during GABAergic interneuron differentiation from each cluster in Dravet Syndrome patients.
D. The tendency of chromatin accessibility during GABAergic interneuron differentiation from each cluster in Dravet Syndrome patients.
E. Expression of the four cluster markers *NANOG* (iPSC; D0), *PAX6* (PNC; D19), *GAD2* (imN; D35) and *BABRG3* (GABA; D65) quantified by qRT-PCR following GABAergic differentiation of control iPSC relative to expression of the housekeeping genes ACTB and GAPDH. Fold change data are presented as log2 [mean ΔΔCT(day Y)] ± SD and individual data points for each cell line are indicated (DS lines in blue: DD1C - square, DD4A - triangle, DD5A – circle please; see Methods for detail).

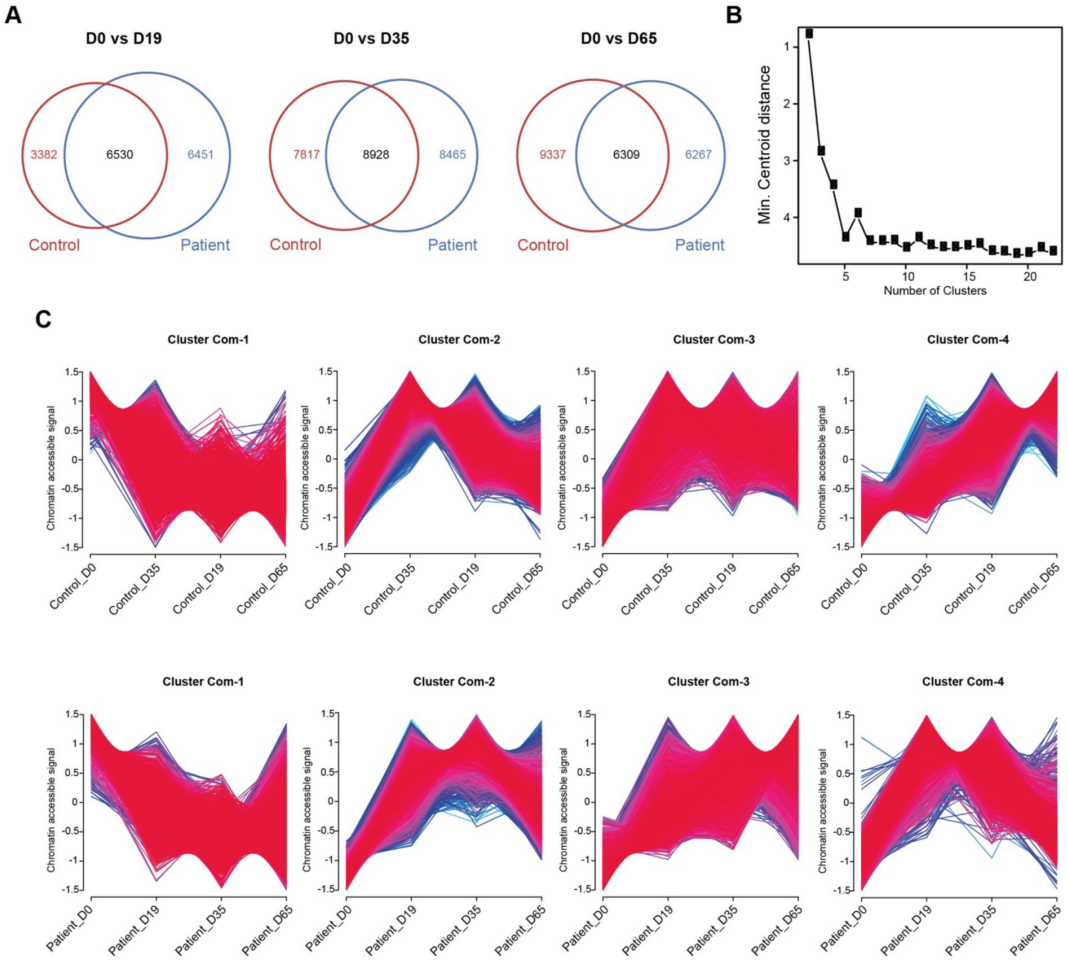

Supplementary Figure 6

Identification of common chromatin accessibility between control and Dravet Syndrome patient iPSCs during GABAergic interneuron differentiation.

A. Venn diagrams showing the shared and distinct accessible chromatin peaks between control and patient samples.

B. Variance with different numbers of clusters derived from common accessible chromatin regions between control and Dravet Syndrome patients.

C. The tendency of chromatin accessibility from common accessible chromatin regions between control and Dravet Syndrome patients during GABAergic interneuron differentiation.

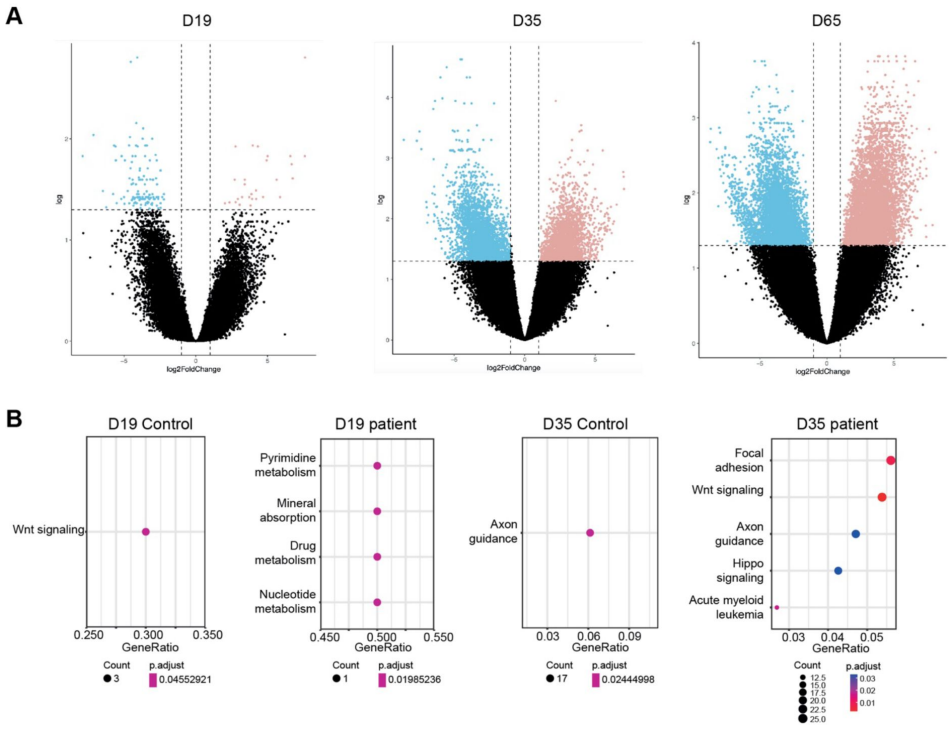

Supplementary Figure 7

Identification of unique accessible chromatin region between control and Dravet Syndrome patient iPSCs during GABAergic interneuron differentiation.

A. Volcano plot of differential accessible chromatin peaks between control and Dravet Syndrome (DS) patients at different stage of differentiation (NPC (Day 19), imN (Day 35) and GABAergic interneuron (Day 65)). Dotted lines indicate cutoff from fold change and false discovery rate.

B. KEGG signal pathway enrichments from unique accessible chromatin region in control and Dravet Syndrome patients at NPC (Day 19), imN (Day 35).

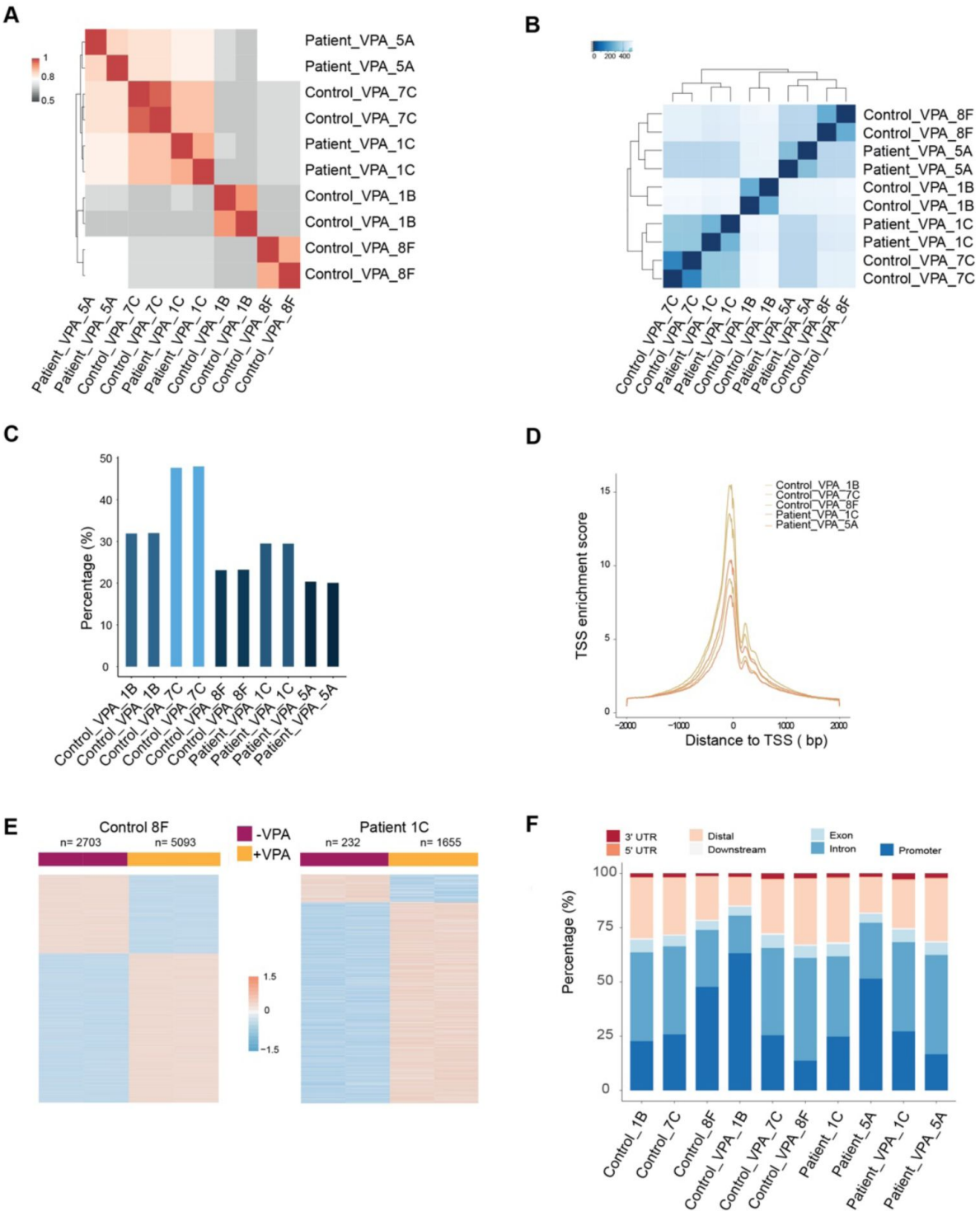

Supplementary Figure 8

Valproic acid treatment reshapes chromatin accessibility of GABAergic interneurons.

A. Pearson correlation matrix from technical duplicates of ATAC-Seq of VPA treated control and Dravet Syndrome patient group.

B. Distance matrix of ATAC-Seq from VPA treated control and Dravet Syndrome patient group.

C. Quantification of fraction of reads in peaks (FRiP) of ATAC-Seq in each condition.

D. Transcription start site (TSS) enrichment score of ATAC-Seq in each sample.

E. Heatmap of differential chromatin accessible regions from VPA non-responsible group, consisting of one control sample and one Dravet Syndrome (DS) patient sample.

F. Genomic distribution of chromatin accessible regions for each individual sample.

References

1 He Z., Li Y., Zhao X., Li B (2022) **Dravet syndrome: Advances in etiology, clinical presentation, and treatment** *Epilepsy Res* **188** https://doi.org/10.1016/j.eplepsyres.2022.107041

2 Dravet C (2011) **The core Dravet syndrome phenotype** *Epilepsia* **52**:3–9 https://doi.org/10.1111/j.1528-1167.2011.02994.x

3 Li W., Schneider A. L., Scheffer I. E (2021) **Defining Dravet syndrome: An essential pre-requisite for precision medicine trials** *Epilepsia* **62**:2205–2217 https://doi.org/10.1111/epi.17015

4 Ragona F (2011) **Cognitive development in children with Dravet syndrome** *Epilepsia* **52**:39–43 https://doi.org/10.1111/j.1528-1167.2011.03000.x

5 Brunklaus A., Zuberi S. M (2014) **Dravet syndrome--from epileptic encephalopathy to channelopathy** *Epilepsia* **55**:979–984 https://doi.org/10.1111/epi.12652

6 Cheah C. S., et al. (2012) **Specific deletion of NaV1.1 sodium channels in inhibitory interneurons causes seizures and premature death in a mouse model of Dravet syndrome** *Proc Natl Acad Sci U S A* **109**:14646–14651 https://doi.org/10.1073/pnas.1211591109

7 Kalume F., et al. (2015) **Sleep impairment and reduced interneuron excitability in a mouse model of Dravet Syndrome** *Neurobiol Dis* **77**:141–154 https://doi.org/10.1016/j.nbd.2015.02.016S0969-9961(15)00043-1

8 Ito S., et al. (2013) **Mouse with Nav1.1 haploinsufficiency, a model for Dravet syndrome, exhibits lowered sociability and learning impairment** *Neurobiol Dis* **49**:29–40 https://doi.org/10.1016/j.nbd.2012.08.003

9 Han S., et al. (2012) **Autistic-like behaviour in Scn1a+/- mice and rescue by enhanced GABA-mediated neurotransmission** *Nature* **489**:385–390 https://doi.org/10.1038/nature11356

10 Yu F. H., et al. (2006) **Reduced sodium current in GABAergic interneurons in a mouse model of severe myoclonic epilepsy in infancy** *Nat Neurosci* **9**:1142–1149 https://doi.org/10.1038/nn1754

11 Tai C., Abe Y., Westenbroek R. E., Scheuer T., Catterall W. A (2014) **Impaired excitability of somatostatin- and parvalbumin-expressing cortical interneurons in a mouse model of Dravet syndrome** *Proc Natl Acad Sci U S A* **111**:E3139–3148 https://doi.org/10.1073/pnas.1411131111

12 Sun Y., et al. (2016) **A deleterious Nav1.1 mutation selectively impairs telencephalic inhibitory neurons derived from Dravet Syndrome patients** *eLife* **5** https://doi.org/10.7554/eLife.13073

13 Schuster J., et al. (2019) **Transcriptomes of Dravet syndrome iPSC derived GABAergic cells reveal dysregulated pathways for chromatin remodeling and neurodevelopment** *Neurobiol Dis* **132** https://doi.org/10.1016/j.nbd.2019.104583

14 Maeda H., et al. (2016) **Establishment of isogenic iPSCs from an individual with SCN1A mutation mosaicism as a model for investigating neurocognitive impairment in Dravet syndrome** *J Hum Genet* **61**:565–569 https://doi.org/10.1038/jhg.2016.5

15 Jiao J., et al. (2013) **Modeling Dravet syndrome using induced pluripotent stem cells (iPSCs) and directly converted neurons** *Hum Mol Genet* **22**:4241–4252 https://doi.org/10.1093/hmg/ddt275

16 Higurashi N., et al. (2013) **A human Dravet syndrome model from patient induced pluripotent stem cells** *Mol Brain* **6** https://doi.org/10.1186/1756-6606-6-191756-6606-6-19

17 Arshad A., et al. (2016) **Extended Production of Cortical Interneurons into the Third Trimester of Human Gestation** *Cereb Cortex* **26**:2242–2256 https://doi.org/10.1093/cercor/bhv074

18 Xu G., et al. (2011) **Late Development of the GABAergic System in the Human Cerebral Cortex and White Matter** *J Neuropath Exp Neur* **70**:841–858 https://doi.org/10.1097/NEN.0b013e31822f471c

19 Allaway K. C., et al. (2021) **Genetic and epigenetic coordination of cortical interneuron development** *Nature* **597**:693–697 https://doi.org/10.1038/s41586-021-03933-1

20 Ogiwara I., et al. (2013) **Nav1.1 haploinsufficiency in excitatory neurons ameliorates seizure- associated sudden death in a mouse model of Dravet syndrome** *Hum Mol Genet* **22**:4784–4804 https://doi.org/10.1093/hmg/ddt331

21 Aras L. M., Isla J., Mingorance-Le Meur A (2015) **The European patient with Dravet syndrome: results from a parent-reported survey on antiepileptic drug use in the European population with Dravet syndrome** *Epilepsy Behav* **44**:104–109 https://doi.org/10.1016/j.yebeh.2014.12.028

22 Ghodke-Puranik Y., et al. (2013) **Valproic acid pathway: pharmacokinetics and pharmacodynamics** *Pharmacogenet Genomics* **23**:236–241 https://doi.org/10.1097/FPC.0b013e32835ea0b2

23 Ximenes J. C. M., Verde E. C. L., Naffah-Mazzacoratti M. G., de Barros Viana G. S. (2012) **Valproic Acid, a Drug with Multiple Molecular Targets Related to Its Potential Neuroprotective Action** *Neuroscience and Medicine* **3**:107–123 https://doi.org/10.4236/nm.2012.31016

24 Balasubramanian D., Pearson J. F., Kennedy M. A (2019) **Gene expression effects of lithium and valproic acid in a serotonergic cell line** *Physiol Genomics* **51**:43–50 https://doi.org/10.1152/physiolgenomics.00069.2018

25 Jiang X., et al. (2019) **Sodium valproate rescues expression of TRANK1 in iPSC-derived neural cells that carry a genetic variant associated with serious mental illness** *Mol Psychiatry* **24**:613–624 https://doi.org/10.1038/s41380-018-0207-1

26 Wang Y., Li Z (2019) **RNA-seq analysis of blood of valproic acid-responsive and non-responsive pediatric patients with epilepsy** *Exp Ther Med* **18**:373–383 https://doi.org/10.3892/etm.2019.7538

27 Golla U., Joseph D., Tomar R. S (2016) **Combined Transcriptomics and Chemical- Genetics Reveal Molecular Mode of Action of Valproic acid, an Anticancer Molecule using Budding Yeast Model** *Sci Rep* **6** https://doi.org/10.1038/srep35322

28 Balasubramanian D., Deng A. X., Doudney K., Hampton M. B., Kennedy M. A (2015) **Valproic acid exposure leads to upregulation and increased promoter histone acetylation of sepiapterin reductase in a serotonergic cell line** *Neuropharmacology* **99**:79–88 https://doi.org/10.1016/j.neuropharm.2015.06.018

29 Schuster J., et al. (2019) **Generation of three human induced pluripotent stem cell (iPSC) lines from three patients with Dravet syndrome carrying distinct SCN1A gene mutations** *Stem Cell Res* **39** https://doi.org/10.1016/j.scr.2019.101523

30 Inoue F., Kreimer A., Ashuach T., Ahituv N., Yosef N (2019) **Identification and Massively Parallel Characterization of Regulatory Elements Driving Neural Induction** *Cell Stem Cell* **25**:713–727 https://doi.org/10.1016/j.stem.2019.09.010

31 Trevino A. E., et al. (2020) **Chromatin accessibility dynamics in a model of human forebrain development** *Science* **367** https://doi.org/10.1126/science.aay1645

32 de la Torre-Ubieta L., et al. (2018) **The Dynamic Landscape of Open Chromatin during Human Cortical Neurogenesis** *Cell* **172**:289–304 https://doi.org/10.1016/j.cell.2017.12.014

33 Inglis G. A. S., et al. (2020) **Transcriptomic and epigenomic dynamics associated with development of human iPSC-derived GABAergic interneurons** *Hum Mol Genet* **29**:2579–2595 https://doi.org/10.1093/hmg/ddaa150

34 Ogiwara I., et al. (2007) **Nav1.1 localizes to axons of parvalbumin-positive inhibitory interneurons: a circuit basis for epileptic seizures in mice carrying an Scn1a gene mutation** *J Neurosci* **27**:5903–5914 https://doi.org/10.1523/JNEUROSCI.5270-06.2007

35 Maroof A. M., et al. (2013) **Directed differentiation and functional maturation of cortical interneurons from human embryonic stem cells** *Cell Stem Cell* **12**:559–572 https://doi.org/10.1016/j.stem.2013.04.008S1934-5909(13)00144-6

36 Strano A., Tuck E., Stubbs V. E., Livesey F. J (2020) **Variable Outcomes in Neural Differentiation of Human PSCs Arise from Intrinsic Differences in Developmental Signaling Pathways** *Cell Rep* **31** https://doi.org/10.1016/j.celrep.2020.107732

37 Stevanovic M., et al. (2021) **SOX Transcription Factors as Important Regulators of Neuronal and Glial Differentiation During Nervous System Development and Adult Neurogenesis** *Front Mol Neurosci* **14** https://doi.org/10.3389/fnmol.2021.654031

38 Lindtner S., et al. (2019) **Genomic Resolution of DLX-Orchestrated Transcriptional Circuits Driving Development of Forebrain GABAergic Neurons** *Cell Rep* **28** https://doi.org/10.1016/j.celrep.2019.07.022

39 Schep A. N., Wu B., Buenrostro J. D., Greenleaf W. J (2017) **chromVAR: inferring transcription-factor-associated accessibility from single-cell epigenomic data** *Nat Methods* **14**:975–978 https://doi.org/10.1038/nmeth.4401

40 Brunklaus A., et al. (2020) **Time to move beyond genetics towards biomedical data-driven translational genomic research in severe paediatric epilepsies** *Eur J Paediatr Neurol* **24**:35–39 https://doi.org/10.1016/j.ejpn.2019.12.001

41 Brunklaus A., et al. (2020) **SCN1A variants from bench to bedside-improved clinical prediction from functional characterization** *Hum Mutat* **41**:363–374 https://doi.org/10.1002/humu.23943

42 Liu Y., et al. (2013) **Dravet syndrome patient-derived neurons suggest a novel epilepsy mechanism** *Ann Neurol* **74**:128–139 https://doi.org/10.1002/ana.23897

43 Inoue Y., et al. (2009) **Stiripentol open study in Japanese patients with Dravet syndrome** *Epilepsia* **50**:2362–2368 https://doi.org/10.1111/j.1528-1167.2009.02179.x

44 Dressler A., et al. (2015) **Efficacy and tolerability of the ketogenic diet in Dravet syndrome - Comparison with various standard antiepileptic drug regimen** *Epilepsy Res* **109**:81–89 https://doi.org/10.1016/j.eplepsyres.2014.10.014

45 Baumann C., Zhang X., Zhu L., Fan Y., De La Fuente R (2021) **Changes in chromatin accessibility landscape and histone H3 core acetylation during valproic acid-induced differentiation of embryonic stem cells** *Epigenetics Chromatin* **14** https://doi.org/10.1186/s13072-021-00432-5

46 Stevanovic M., et al. (2021) **SOX Transcription Factors as Important Regulators of Neuronal and Glial Differentiation During Nervous System Development and Adult Neurogenesis** *Front Mol Neurosci* **14** https://doi.org/10.3389/fnmol.2021.654031

47 Sobol M., et al. (2015) **Methods of Reprogramming to Induced Pluripotent Stem Cell Associated with Chromosomal Integrity and Delineation of a Chromosome 5q Candidate Region for Growth Advantage** *Stem Cells Dev* **24**:2032–2040 https://doi.org/10.1089/scd.2015.0061

48 Chen X., et al. (2016) **ATAC-see reveals the accessible genome by transposase-mediated imaging and sequencing** *Nat Methods* **13**:1013–1020 https://doi.org/10.1038/nmeth.4031

49 Buenrostro J. D., Giresi P. G., Zaba L. C., Chang H. Y., Greenleaf W. J (2013) **Transposition of native chromatin for fast and sensitive epigenomic profiling of open chromatin, DNA-binding proteins and nucleosome position** *Nat Methods* **10**:1213–1218 https://doi.org/10.1038/nmeth.2688

50 Langmead B., Trapnell C., Pop M., Salzberg S. L (2009) **Ultrafast and memory-efficient alignment of short DNA sequences to the human genome** *Genome Biol* **10** https://doi.org/10.1186/gb-2009-10-3-r25

51 Zhang Y., et al. (2008) **Model-based analysis of ChIP-Seq (MACS)** *Genome Biol* **9** https://doi.org/10.1186/gb-2008-9-9-r137

52 Ramirez F., Dundar F., Diehl S., Gruning B. A., Manke T (2014) **deepTools: a flexible platform for exploring deep-sequencing data** *Nucleic Acids Res* **42**:W187–191 https://doi.org/10.1093/nar/gku365

53 Robinson M. D., McCarthy D. J., Smyth G. K (2010) **edgeR: a Bioconductor package for differential expression analysis of digital gene expression data** *Bioinformatics* **26**:139–140 https://doi.org/10.1093/bioinformatics/btp616

54 Love M. I., Huber W., Anders S (2014) **Moderated estimation of fold change and dispersion for RNA-seq data with DESeq2** *Genome Biol* **15** https://doi.org/10.1186/s13059-014-0550-8

55 Futschik M C. B (2005) **Noise robust clustering of gene expression time-course data** *Journal of Bioinformatics and Computational Biology* :965–988

56 Yu G., Wang L. G., He Q. Y (2015) **ChIPseeker: an R/Bioconductor package for ChIP peak annotation, comparison and visualization** *Bioinformatics* **31**:2382–2383 https://doi.org/10.1093/bioinformatics/btv145

57 Yu G. C., Wang L. G., Han Y. Y., He Q. Y (2012) **clusterProfiler: an R Package for Comparing Biological Themes Among Gene Clusters** *Omics* **16**:284–287 https://doi.org/10.1089/omi.2011.0118

58 Heinz S., et al. (2010) **Simple combinations of lineage-determining transcription factors prime cis-regulatory elements required for macrophage and B cell identities** *Mol Cell* **38**:576–589 https://doi.org/10.1016/j.molcel.2010.05.004

Editors

Reviewing Editor
Sacha Nelson
Brandeis University, Waltham, United States of America

Senior Editor
Detlef Weigel
Max Planck Institute for Biology Tübingen, Tübingen, Germany

Reviewer #2 (Public Review):

Summary:

Overall this is an interesting innovative study that examines chromatin accessibility in an inhibitory iPSC model of Dravet Syndrome. The authors detect a potential intriguing development defect in the patient-specific neurons, however the correlation with gene expression or protein abundance is not compelling and the variability of the data is still difficult to determine.

Strengths:

(1) This is a novel and interesting study that aims to investigate the epigenetic changes that occur in a sodium channel model of epilepsy, these are oft ignored, but also an interesting area for future therapeutics.

(2) The paper is well written with good graphics and flow.

(3) With caveats noted below, there is an intriguing developmental defect in GABAergic neuron differentiation in this model. It would be interesting to see how this correlated with the expression of SCN1A, and I was surprised this was not addressed in the manuscript via RNA/protein abundance, nor how the absence of a sodium channel can accelerate differentiation when a priori I might expect the opposite (as less 'neuronal' signal)

(4) There is exploratory analysis that VPA alters chromatin accessibility at an individual-specific level. Though it was not noted if any of the DS patients,

Weaknesses addressed:

(1) Representative images for cell-identity markers are now shown for D19 and D65.

(2) The methods now state that three differentiations were performed.

(3) The authors address a possible role for cell death in data obtained from their cultures by assessing viability with trypan blue staining.

(4) Some features of ATAC signal normalization and enrichment analysis have been better documented.

(5) Some of the variability in key results is better documented.

Weaknesses poorly or not addressed:

(1) Although the authors include prior RNAseq data and report on qPCR measurements for SCN1A (Supp Fig 1)these do not on the surface appear to agree, with the RNAseq showing little apparent difference between patients and controls, while the qPCR seems to show a two-fold difference at D65. This is likely a misleading artifact of normalizing PCR expression to that at D0 when the gene is not expressed but has mildly different low levels in patients and controls. No measurement of the protein product or its function is included. This is a major weakness that casts doubt on the core hypothesis that epigenetic changes play a key causal role in Dravet syndrome.

(2) Although some QC on ATAC is described, QC performed on iPSC lines, i.e. karyotype/CNV analysis and confirmation of genotypes is not described in the paper.

(3) The authors describe a method for trying to diminish variability but do not adequately explain this method or how much variability remains in many of their measures.

(4) Given that VPA would be administered in patients with fully mature inhibitory neurons, it is difficult to determine the biological relevance of these findings.

https://doi.org/10.7554/eLife.92599.2.sa1

Author response:

The following is the authors' response to the original reviews.

> ***Public Review:***
>
> *This study used ATAC-Seq to characterize chromatin accessibility during stages of GABAergic neuron development in induced pluripotent stem cells (iPSCs) derived from both Dravet Syndrome (DS) patients and healthy donors. The authors report accelerated GABAergic maturation to a point, followed by further differentiation into a perturbed chromatin profile, in the cells from patients. In a preliminary analysis, valproic acid, an anti-seizure medication commonly used in patients with DS, increased open chromatin in both patient and control iPSCs in a nonspecific manner, and to different degrees in cultures derived from different patients. These findings provide new information about DS-associated changes in chromatin, and provide further evidence for developmental abnormalities in interneurons with DS.*
>
> *Strengths:*
>
> *This is a novel study that aims to investigate the epigenetic changes that occur in a sodium channel model of epilepsy; these changes are often ignored but may be an*

> *interesting area for future therapeutics. In general, the flow of the paper is good, and the figures are well-designed. Reply: Thank you for your positive feedback about our work.*
>
> *Weaknesses:*
>
> *The most substantial weakness relates to the observation that DS is often viewed as a monogenic form of epilepsy. It is directly linked to SCN1A gene haploinsufficiency (Yu et al, 2006; Ogiwara et al, 2007). The gene product is Nav1.1, the alpha subunit of voltage-gated sodium channel type I that regulates neuronal excitability. Yet, analysis was conducted at time points of GABAergic interneuron differentiation in which SCN1A is likely not expressed. The paper would be strengthened if SCN1A expression and Nav1.1 protein were examined across the experimental time course. If SCN1A is not yet expressed, this would complicate any explanation of how the observed epigenetic changes might arise. It also seems counterintuitive that the absence of a sodium channel can accelerate differentiation, when, a priori, one might expect the opposite (a 'less neuronal' signal).*

Thanks, this is an important point! In our revised manuscript, we have incorporated data on the expression of *SCN1A* at d19 and d65 of GABAergic development in both the control and patient groups. We first retrieved data from our previous RNA-Seq analysis, showing *SCN1A* gene expression in our cells at both d19 and d65. We have now updated our text on the *SCN1A* gene expression in the revised manuscript (Revised Supplementary Figure 1A, revised text Line 108-109). Second, we confirmed the dynamics of *SCN1A* expression by real-time quantitative RT/PCR analysis at four time-pionts of GABAergic development (d0, d19, d35 and d65). Notably, expression of *SCN1A* was detected by qRT-PCR from d19 and the expression increased with differentiation. We have now included this information in the revised manuscript (Revised Supplementary Figure 1B, revised text Line 112).

> *Related to this, another important limitation of the study is that the controls are cells derived from healthy individuals and not from isogenic lines. The usage of isogenic lines is extremely relevant for every study in which iPSC-derived somatic cells are used to model a disease, but specifically in diseases like DS, in which the genetic background has an ascertained impact on disease phenotype (Cetica et al, 2017 and others). This serious limitation should be considered.*

Yes, we fully agree that isogenic and edited patient-derived iPSC would have been the ideal controls. At an early stage we therefore invested considerable time and efforts in order to generate isogenic lines from patientderived iPSC. However, editing of the *SCN1A* variants in patient-derived iPSC turned out unsuccessful after several trials and modifications so we finally turned to iPSC from healthy donors. This is now discussed together with other limitations of our study in the revised manuscript (end of discussion section, lines 499-506).

> *In addition, the authors should provide data on variability across cell lines and differentiations to help convince the reader that the results can be attributed to genetic defects, rather than variability across individuals.*

This is a valuable point. In the revised manuscript, we have now added plots and IF staining from individual samples to give the readers a complete picture on how they are distributed (Revised Supplementary Figure 1C, Revised Supplementary Figure 2, and Revised Supplementary Figure 4).

In the revised manuscript, we incorporated an explanation on the strategy used to compare the two groups (cases *vs*. controls) in more detail. In our analysis, we first compared the dynamic changes of chromatin accessibility cell line by cell line across differentiation. We then extracted the common changes from different cell lines at each time point (Revised text

line 152-155, line 226-228). Using this strategy, we extracted the common changes confined to the control and patient groups, respectively. With this approach we avoid to capture the variability across individuals.

> *Additionally, the authors acknowledge the variability of the differentiations and cell lines, which is commendable, and they attribute this to "possibly reflecting cell line specific and endogenous differences reported previously", but could also have to do with cell death. This is a large confounding factor for ATAC-seq. Certainly, Sup Fig 1C shows lower FrIP scores, consistent with cell death, and there seems to be a lot of death in the representative images. Moreover, the iGABA neurons are very difficult to keep alive, especially to 65 days, without co-culturing with glia and/or glutamatergic neurons. The authors should comment on how much these factors may have influenced their results.*

With this point in mind, we re-examined QC of our ATAC-Seq across all samples: As shown in revised

Supplementary Figure 2C and Supplementary Figure 4C, our cutoff for FRiP is 15%, and all of samples have an FrIP of more than 15%. At the later time points (d35 or d65), we did not observe a FRiP <15%. We therefore feel confident that the quality of ATAC-Seq is good enough for downstream analysis and data interpretation.

Regarding the differentiation protocol, we are following a directed protocol of iPSC towards interneurons. The protocol is described in detail by Maroof et al (reference 34) and slightly modified in our lab (described in reference 13). With our modified protocol, GABAergic cells are viable beyond day 65 without the need of co-cultures with astrocyte or microglia. This is also reflected by the electrophysiological activity of interneurons at d65 and at later time points (reference 13). Additionally, our ambition was to obtain a homogeneous cell population for further analysis. Adding other cell types to the cultures would have interfered with downstream processes and a need for cell sorting. Using our protocol, we obtain viable GABA interneurons after up to 100 days in culture. To assess the viability of our cells at the point of sampling (other than by morphological assessment), we used Trypan blue staining and an automated cell counter. Only samples with a viability >90% were processed for ATAC seq. which is a commonly used cut-off for cell viability. We have now modified the method section in the revised version to describe the GABAergic differentiation and sampling (line 519-529).

> *Finally, changes in gene expression are only inferred, as no RNA levels were measured. If RNA-seq was not possible it would have been good to see at least some of the key genes/findings corroborated with RNA/protein levels vs chromatin accessibility alone, particularly given that these molecular readouts do not always correlate.*

In our revised manuscript, we include our recently published RNA-seq performed at d19 and d65. We also correlated the RNAseq and ATACseq data obtained from the same samples. The Pearson correlations between gene expression and chromatin accessibility were within the range 0.49-0.57 (Revised Supplementary Figure 2G, Revised supplementary Figure 4G), which is acceptable according to standard criteria. The results confirmed that the quality of ATAC-Seq is good enough for analysis of expression levels and chromatin openness in key genes. We also added gene expression levels from RNA-seq (d19 and d65) in our revised manuscript (Revised Figure 1G, Revised Figure 2G). Finally, we performed qRT-PCR analysis of key genes in each cluster and the results are now included in the revised version (Revised Supplementary Figure 3E, Revised Supplementary Figure 5E)

> *Additional Points:*

> *(1) Representative images for cell-identity markers for only D65 are shown, and not D0, D19, and D35 though it is stated in the text that this was performed. At a minimum, these representative images should be shown for all lines.*

As suggested, we have now added images for cell identity markers of all iPSC lines in the revised version (Revised Supplementary Figure 1C).

> *(2) What QC was performed on iPSC lines, i.e. karyotype/CNV analysis and confirmation of genotypes?*

All iPSC lines used in this study have been fully characterized according to standard and state-of-the art procedures: Expression of pluripotency and stemness genes has been shown by immunostaining, flow cytometry and scorecard analysis; integrity of the genome has been assessed by karyotyping using g-banding; differentiation capacity was characterized using an embryoid body assay in combination with scorecard analysis; and genotypes were verified by Sanger sequencing. Please, see the following publications for full datasets: Schuster et all, Neurobiol Dis 2019, Schuster et al Stem Cell Res 2019, Sobol et al Stem Cells and Development 2015. In our lab, the integrity of iPSC lines are routinely verified using flow cytometry (expression for TRA-1-60 and SSEA4), immunostaining (expression of NANOG, SOX2 and OCT4), Sanger sequencing (targeting variants in SCN1A gene), cell morphology analysis and analysis of mycoplasma by MycoAlert® (Lonza).

> *(3) Were all experiments performed on a single differentiation? Or multiples? Were the differentiations performed with the same type? If not, was batch considered in the analysis?*

Thank you for raising this question. The text Material and Methods has been modified as follows, to better describe the differentiation and sampling procedure:

“GABAergic interneuron differentiation from iPSCs was performed as previously described (reference 13). The protocol utilizes DUAL SMAD inhibition to induce neurogenesis towards neural stem cells for 10 days, followed by patterning with high levels of sonic hedgehog for nine days towards cortically fated neuronal progenitor cells (NPC) and subsequent maturation for 46 days, i.e. a total of 65 days (Figure 1A). Neuronal cells at day 65 and onwards are healthy and viable as judged by morphological assessment by light microscopy. *Differentiation was performed at least 3 times per cell line.*

Cell cultures were sampled at days 0 (D0), D19, D35 and D65, respectively, by harvesting cells with TryplE and centrifugation (300 x g, 3 min). Harvested cells were counted and assessed for viability using trypan blue staining and an automated EVE cell counter (Nano Entek). Samples with a viability of >90% were chosen for ATAC-Seq library preparation (see below).”.

> *I also assume that technical replicates were merged, and then all three biological replicates were kept for each analysis and outliers were not removed, e.g. Control_D19_8F seems like an example of an outlier.*

This is a valuable point. We agree on that there is variability across three health donors and patients, respevtively, but the quality of ATAC-Seq is good after multiple assessment of QC (Revised Supplementary Figure 2B-D). The color code in Supplementary Figure 1C may be mis-leading as the Pearsson correlation of all samples was displayed. Overall, the correlation from all ATAC-seq among replicates are over 0.8. At the same time, we observed that samples at d0 are clustered together, but not at the later time points. We interpret this as related to the cell-line specific plasticity of chromatin dynamic during differentiation. The observation agrees with our results from PCA (Revised Supplementary Figure 2F).

> *(4) In Figure 1C, it is intriguing that the ATACseq signal gets stronger in imN. One might expect it to be strongest in the iPSCs which are undifferentiated and have the highest levels of open chromatin. Is this a function of sequencing depth, or are all the Y-axes normalized across all time points?*

This is another valuable point. Figure 1C present the average chromatin openness for clusters specific regions- not of chromatin openness from the entire genome, which is a reason for why the chromatin openness at

D35 is higher than at other time-points. The genome-wide chromatin openness is presented in revised

Supplementary Figure 2D and we have now updated the figure legend to avoid any potential misunderstanding.

The sequencing depth for each sample is extracted in a similar range. To give the readers a complete picture, we also present the depth of sequencing reads for each sample (Revised Supplementary Figure 2A and Revised Supplementary Figure 4A). The Y-axes of genome browser tracks were normalized, and we added the normalized value in the figures.

> *(5) In Figure 1F, are these all enriched terms, or were they prioritized somehow?*

Yes, the enriched terms are prioritized based on biological meanings, and we have now clarified this in the updated legend of the manuscript. In addition, all enriched terms are now included in revised Supplementary Table 2 and Supplementary Table 4.

> *(6) In Figure 1G (also the same plots in Fig 2/3), are all these images normalized i.e. there is no scale bar for each track, and do they represent and aggregate BAM/bigwig?*

Yes, the genome browser tracks were normalized and we have now revised the figures by adding scale bars.

> *It would be good to show in supplement the variability across cell lines/diffs - particularly given the variability in the heatmap/PCA - and demonstrate the rigor/reproducibility of these results. This comment applies to all these plots across the 3 figures, particularly as in some instances the samples appear to cluster by individual first and then time point (Sup Fig 3B).*

Thanks. We have now revised the figure with plots showing individual samples.

> *How confident are the authors that these effects are driven by genotype and not a single cell line? In the Fig 3D representation of NANOG, it is very difficult to see any difference between patient and control.*

In Figure 3D, we showed *common* chromatin dynamics in the control and patient groups. To avoid any misunderstanding, we have now updated our legend in the revised manuscript.

> *(7) For the changes in occupancy annotation (UTR/exon/intron etc), are these differences still significant after correcting for variability from cell line to cell line at each time point? I.e. rather than average across all three samples, what is the range? Reply: Revised accordingly.*
>
> *(8) The VPA timepoint is not well-justified. Given that VPA would be administered in patients with fully mature inhibitory neurons, it is difficult to determine the biological*

> *relevance. I appreciate that this is a limitation of the model, but this should at least be addressed in the manuscript.*

We agree on that our model system of GABAergic interneuron development has limitations and that cells may not fully recapitulate the development and physiology *in vivo*. Obvious factors to consider in our system are the directed protocol to enrich for GABAergic interneurons and the differentiation time-line restricted to 65d. This is now discussed (lines 499-506).

> ***Recommendations for the authors:***
>
> *(1) The term 'mutation' has been replaced with the term ' pathogenic variant' or likely pathogenic variant depending on the context, please see PMID: 25741868*

Thank you for pointing this out. We have replaced all instances of “mutation” with “pathogenic variant” throughout the manuscript.

> *(2) It is unclear what the nomenclature for sample labelling is in Supplementary Figure 1, e.g. 7C, 8F, 1B.*

We apologize for this confusion. There are cell lines names. We labeled all data and images according to cell line name, i.e. control lines: Ctl1B, Ctl7C and Ctl8F; patient lines: DD1C, DD4A, DD5A. To avoid any potential confusion, we have added a note in the revised legend of Supplementary Figure 1B.

> *(3) Can the authors confirm that the Deseq2 FDR values are Benjamini-Hochberg procedure corrected per default settings? If so, this should ideally be added to methods or legend for clarity*

Yes, default settings were used in Deseq2 FDR values, which is added in the method part of revised manuscript.

> *(4) While it makes sense that the authors present the data in the order of Figure 1, and Figure 2, this actually makes it quite difficult to compare the two datasets, especially for the functional enrichment in the "F" figures. It may be helpful to consider re-organizing the figure order. For instance, for the long-term potentiation signal in the DS-iPSCs, what does this mean in terms of biological relevance? Or maybe Figure 2 needs to be supplementary given that Figure 3 is a more direct comparison.*

Thank you for the suggestions. We attempted to reorganize during our revision. We still believe it is easier for the audience to grasp the main message if we organize it according to our current workflow—first presenting an individual differential landscape for controls and patients, and then comparing the common and unique aspects among them.

https://doi.org/10.7554/eLife.92599.2.sa0